Inhomogeneous Poisson Sampling of Finite-Energy Signals With Uncertainties in $\mathbb{R}^d$

Flavio Zabini, *Member, IEEE*, and Andrea Conti, *Senior Member, IEEE*

***Abstract*—Spatiotemporal signal reconstruction from samples randomly gathered in a multidimensional space with uncertainty is a crucial problem for a variety of applications. Such a problem generalizes the reconstruction of a deterministic signal and that of a stationary random process in one dimension, which was first addressed by Whittaker, Kotelnikov, and Shannon. In this work we analyze multidimensional random sampling with uncertainties jointly accounting for signal properties (signal spectrum and spatial correlation) and for sampling properties (inhomogeneous sample spatial distribution, sample availability, and non-ideal knowledge of sample positions). The reconstructed signal spectrum and the signal reconstruction accuracy are derived as a function of signal and sampling properties. It is shown that some of these properties expand the signal spectrum while others modify the spectrum without expansion. The signal reconstruction accuracy is first determined in a general case and then specialized for cases of practical interests. The optimal interpolator function is derived and asymptotic results are obtained to show the impact of sampling non-idealities. The analysis is corroborated by verifying that previously known results can be obtained as special cases of the general one and by means of a case study accounting for various settings of signal and sample properties.**

***Index Terms*—Multidimensional random sampling, signal reconstruction, inhomogeneous Poisson point process, crowdsourcing, sampling uncertainty.**

I. Introduction

MULTIDIMENSIONAL reconstruction of signals is a key enabler for emerging applications in various sectors including array signal processing, magnetic resonance imaging, seismology, digital communication and control, software defined radio and networks, vehicular networks, and environmental monitoring [1]–[12]. Big data [13]–[15] and crowdsourcing [16]–[19] applications can be associated with multidimensional random sampling (e.g., to reconstruct spatial distribution of data).

Classical problems in one dimension are the reconstruction of a deterministic signal and that of a stationary random process from a finite or an infinite number of its samples [20]. On the one hand, the uniform sampling theorem from Whittaker-Kotelnikov-Shannon [21]–[23] states that a signal can be exactly reconstructed from its samples if the sampling frequency is at least twice the signal bandwidth (Nyquist rate). On the other hand, random sampling introduces non-uniformities and uncertainties that challenges the signal reconstruction. The most important result in deterministic irregular sampling is the one by Landau [24], who found necessary conditions on the samples density for exact reconstruction of a finite-energy bandlimited signal. Such a result has been generalized for multidimensional domain in [25]. The signal spectrum reconstruction from samples randomly scattered in time according to a stationary Poisson point process (PPP)[1] was analyzed in [27], showing that the signal spectrum can be reconstructed if the sampling process intensity is greater than or equal to the Nyquist rate for uniform sampling. In such a case, the spectrum of the reconstructed signal has an additional white noise component due to sampling randomness.

Multidimensional random sampling has recently attracted a vast interest due to various applications in sensor networks where a signal reconstruction entity collects samples from sensors randomly scattered in an environment [28]–[36]. Existing works focus on algorithms aiming to improve the reconstruction accuracy in multidimensional domain, for instance using quantized spatially correlated data and fusion-center feedback [37], observation prediction [38], spatial best linear unbiased estimation [39], or spatial Gaussian process regression [40]. Other works extends Marvasti's approach or its main assumption (stationary PPP) to the multidimensional domain (homogeneous PPP) [41]–[47]. The presence of signal sources scattered according to a homogeneous PPP is also common in recent works on wireless communication and localization networks [48]–[52].

However, homogeneous point processes do not always accurately describe the sample spatial distribution in many cases of interest (e.g., sensors scattered accordingly to different densities in regions of a monitored area). Moreover, in real scenarios there might be uncertainties due to imperfect knowledge of sample location information. Such uncertainties can be detrimental for signal reconstruction and call, together with inhomogeneous sample spatial distribution, for a new methodology to analyze multidimensional random sampling.

Lacaze solved the one-dimensional problem for cases in which the sampling time is observed or unknown [53]. In the former case, an extension of the Lagrange interpolation formula [20] was given, while in the latter the signal estimator was provided for Gaussian distributed jitter of regular sampling time.[2] The extension of the analysis to a d-dimensional space when

Manuscript received May 29, 2015; revised December 28, 2015; accepted March 22, 2016. Date of publication April 11, 2016; date of current version July 25, 2016. The associate editor coordinating the review of this manuscript and approving it for publication was Prof. Subhrakanti Dey. This research is supported in part by the Italian MIUR project GRETA under Grant 2010WHY5PR.

F. Zabini is with DEI and WiLab, University of Bologna, and IEIIT/CNR, Bologna 40100, Italy (e-mail: flavio.zabini.it@ieee.org).

A. Conti is with ENDIF, University of Ferrara, Ferrara 44100, Italy (e-mail: a.conti@ieee.org).

Color versions of one or more of the figures in this paper are available online at http://ieeexplore.ieee.org.

Digital Object Identifier 10.1109/TSP.2016.2552499

[1] In the case of PPP, the term *stationary* is used for the time domain, while *homogeneous* is widely adopted for multidimensional domain [26].

[2] The signal reconstruction accuracy, in terms of reconstruction mean-square error (MSE), is typically obtained by first evaluating the MSE conditioned on the samples position and then averaging over sample spatial distribution. This typically results in cumbersome expressions for the signal reconstruction MSE, as Lacaze also noticed for the one-dimensional case [54].

sample positions are randomly distributed according to an inhomogeneous point process and are not perfectly known is not straightforward. A sampling theorem for non-stationary random process (non-stationarity is referred to the signal to be reconstructed) has been presented by Gardner in a two-dimensional domain [55], and then generalized by Sharma and Mehta to the multidimensional case [56]. The case of a non-stationary sampling process (non-stationarity is here referred to the sampling process) is still an open problem. Inhomogeneous distribution of wireless nodes according to a modified Ginibre point process is considered in [57] for communication among nodes with repulsive scattering in $\mathbb{R}^2$. However this kind of distribution implicitly assumes a circular symmetry that well fits cellular scenarios, but can be less appropriate in other applications, such as those based on sensor networks. We consider a general scenario where the sample spatial distribution depends on external causes and is not tailored to the sampled signal (e.g., applications to environmental sensing [41] and network interference characterization [48]). Therefore, emerging approaches such as compressed sensing [58]–[60] can be unsuitable in such conditions. A framework for the analysis of inhomogeneous multidimensional random sampling without making any strong assumption on the sampled signal (e.g., sparse representation) is missing in the literature. In [61] a geometrical approach to reconstruct a signal from arbitrary samples in time is proposed and reconstruction error bounds are provided, but its application to a multidimensional spatial domain is not straightforward.

This paper analyzes the reconstruction of a finite-energy signal (e.g., the instantiation of a random process in a finite space) from samples randomly gathered with uncertainties in $\mathbb{R}^d$ according to an inhomogeneous Poisson sampling process (PSP). The reconstructed signal spectrum and the signal reconstruction accuracy are derived as a function of both the signal properties (signal spectrum and spatial correlation) and sampling properties (inhomogeneous spatial distribution, sample availability, and non-ideal knowledge of sample positions). For the reconstructed signal spectrum, we determine the properties that expand the spectrum and those that modify it in-band (whose effects can thus be compensated by proper filtering). For the signal reconstruction, we determine the reconstruction accuracy for an omnicomprehensive case by directly evaluating the unconditioned MSE in closed-form. In addition, the optimal linear space-invariant (LSI) interpolator[3] expression is determined and asymptotic MSE expressions (for large sampling process intensity with respect to the signal band cardinality) are derived. It will be shown that previously known results can be obtained as corollaries of the proposed theorems. A case study accounting for various signal and sample properties also corroborates the analysis.

The remainder of the paper is organized as in the following. Section II presents the sampling process and the uncertainties models. Section III describes the signal reconstruction and provides theorems and corollaries for both the reconstructed signal spectrum and the reconstruction MSE. Section IV analyzes the interpolation filtering. Section V shows results for a case study. Final remarks are given in Section VI.

[3]In a multidimensional domain the term *space-invariant* takes the place of the usual term *time-invariant* in the time-domain.

TABLE I
MAIN QUANTITIES AND OPERATORS USED THROUGHOUT THE PAPER

Quantity	Significance
$\mathbf{\Pi}$	Poisson point process in $\mathbb{R}^d$
$\mathcal{A}$	sampling space
$N_\Pi(\mathcal{A})$	cardinality of $\mathbf{\Pi} \cap \mathcal{A}$ (counting measure)
$\mathbf{x}$, $\boldsymbol{\nu}$	spatial position and spatial frequency in $\mathbb{R}^d$
$z(\mathbf{x})$, $Z(\boldsymbol{\nu})$	signal to be reconstructed and its Fourier transf.
$\mathbf{x}_n$	n-th sample position in $\mathbf{\Pi}$
$\mathcal{C}_\ell^{(d)}$	hypercube in $\mathbb{R}^d$ centered at $\mathbf{0}$ with side 2ℓ
$\mathcal{N}_\mathbf{\Pi}$, $\mathcal{N}_\ell$	index set of samples in $\mathbf{\Pi}$ and in $\mathbf{\Pi} \cap \mathcal{C}_\ell^{(d)}$
E_z	energy of $z(\mathbf{x})$
$\mathcal{S}(\mathbf{x})$, $\mathcal{L}(\mathbf{x})$	random sampling process w/o and with losses
$\mu_\mathcal{S}(\mathbf{x})$, $\mu_\mathcal{L}(\mathbf{x})$	expectation of $\mathcal{S}$ and $\mathcal{L}$
$R_\mathcal{S}(\mathbf{x},\boldsymbol{\tau})$, $R_\mathcal{L}(\mathbf{x},\boldsymbol{\tau})$	autocorrelation function of $\mathcal{S}$ and $\mathcal{L}$
$\mathcal{U}_\mathcal{S}(\boldsymbol{\nu})$, $\mathcal{U}_\mathcal{L}(\boldsymbol{\nu})$	Fourier transf. of $\mu_\mathcal{S}(\mathbf{x})$ and $\mu_\mathcal{L}(\mathbf{x})$
$\mathtt{z}_\mathcal{S}(\mathbf{x})$, $\mathtt{z}_\mathcal{L}(\mathbf{x})$	signal sampled according to $\mathcal{S}$ and $\mathcal{L}$
$\mathcal{E}_z(\boldsymbol{\nu})$	energy spectral density of $z(\mathbf{x})$
$\mathcal{E}_{\mathtt{z}_\mathcal{S}}(\boldsymbol{\nu})$, $\mathcal{E}_{\mathtt{z}_\mathcal{L}}(\boldsymbol{\nu})$	energy spectral density of $\mathtt{z}_\mathcal{S}(\mathbf{x})$ and $\mathtt{z}_\mathcal{L}(\mathbf{x})$
$\lambda(\mathbf{x})$, $\overline{\lambda}$	local and average intensity of $\mathbf{\Pi}$
$R_\lambda(\boldsymbol{\tau})$	autocorrelation function of $\lambda(\mathbf{x})$
$\Lambda(\boldsymbol{\nu})$	Fourier transf. of $\lambda(\mathbf{x})$
$W_\lambda(\boldsymbol{\nu})$	Fourier transf. of $R_\lambda(\boldsymbol{\tau})$
$q(\mathbf{x})$	probability of sample availability at $\mathbf{x}$
q_n	probability of n-th sample availability
$\overline{q}$	average probability of sample availability
$\hat{\mathbf{x}}_n$	estimated position of the n-th sample
$\mathbf{e}_\mathrm{s}(\mathbf{x}_n)$	position error for the n-th sample
$\sigma^2_{\mathbf{e}_\mathrm{s}}$	sample position error variance
$\theta(\mathbf{x})$	interpolation function in $\mathbb{R}^d$
$\Theta(\boldsymbol{\nu})$	Fourier transf. of $\theta(\mathbf{x})$
κ_θ	interpolator parameter
B	signal bandwidth per dimension
B_λ, B_q	bandwidth per dimension of $\lambda(\mathbf{x})$ and $q(\mathbf{x})$
B_s	reconstructed signal bandwidth per dimension
$\mathcal{B}$, $\mathcal{B}_\theta$	signal and interpolator band in $\mathbb{R}^d$
ι_λ, $\iota_{\mathcal{B}_\theta}$	oversampling for intensity and spatial band
ε_s	normalized signal reconstruction MSE
$(f * g)(\mathbf{u})$	convolution of functions f and g at $\mathbf{u}$
$\mathbf{a} \cdot \mathbf{b}$	scalar product of vectors $\mathbf{a}$ and $\mathbf{b}$
$\breve{\phi}$	normalized quantity from ϕ
$z^\dagger$	complex conjugate of $z \in \mathbb{C}$
$\mathbb{E}\{\cdot\}$	statistical expectation
$\delta(\cdot)$	Dirac delta generalized function
$\mathbb{1}_\mathcal{A}(\mathbf{x})$	indicator function for $\mathbf{x} \in \mathcal{A}$
$\lvert\cdot\rvert$	Lebesgue measure of a subset in $\mathbb{R}^d$
$f_\mathtt{e}(\cdot)$, $\Phi_\mathtt{e}(\cdot)$	PDF of RV $\mathtt{e}$ and its Fourier transf.
$\boldsymbol{\mathcal{F}}\{\cdot\}(\cdot)$, $\boldsymbol{\mathcal{W}}_t\{\cdot\}(\cdot)$	Fourier and t-Weierstrass transforms in $\mathbb{R}^d$
$\boldsymbol{\mathcal{M}}_{\sigma,\varphi}\{\cdot\}$	φ-mean with parameter σ

Notations: Quantities and operators used throughout the paper are reported in Table I.

II. MULTIDIMENSIONAL RANDOM SAMPLING MODEL

We now model the observed multidimensional signal and describe the sampling process. A simple example is also provided for clarification of each considered aspect.

A. Multidimensional Signal

Consider a multidimensional signal $w(\mathbf{x}) \in \mathbb{C}$, instantiation of the observed process $\mathtt{w}(\mathbf{x})$ at position $\mathbf{x} \in \mathbb{R}^d$, with spatial frequency band $\mathcal{B}_\mathtt{w} \subset \mathbb{R}^d$ of cardinality $|\mathcal{B}_\mathtt{w}|$.[4] Let $z(\mathbf{x}) \triangleq w(\mathbf{x})\mathbb{1}_\mathcal{A}(\mathbf{x})$ be the truncated version of $w(\mathbf{x})$, in $\mathcal{A} \subseteq \mathbb{R}^d$ with Fourier transform (FT) $Z(\boldsymbol{\nu}) \triangleq \boldsymbol{\mathcal{F}}\{z(\mathbf{x})\}(\boldsymbol{\nu}) = \int_{\mathbb{R}^d} z(\mathbf{x}) e^{-\jmath 2\pi \boldsymbol{\nu}\cdot\mathbf{x}} d\mathbf{x}$ and finite energy E_z. By defining the

[4]The maximal bandwidth-per-dimension is $B_\mathtt{w} \triangleq \min\{\ell : \mathcal{B}_\mathtt{w} \subseteq \mathcal{C}_\ell^{(d)}\}$, where $\mathcal{C}_\ell^{(d)} \triangleq \{\boldsymbol{\nu} : \prod_{i=0}^{d-1} \mathrm{rect}(\frac{\nu_i}{2\ell}) > 0\}$ and $\mathrm{rect}(x) \triangleq 1$ for $|x| \leq 1/2$ and 0 otherwise.

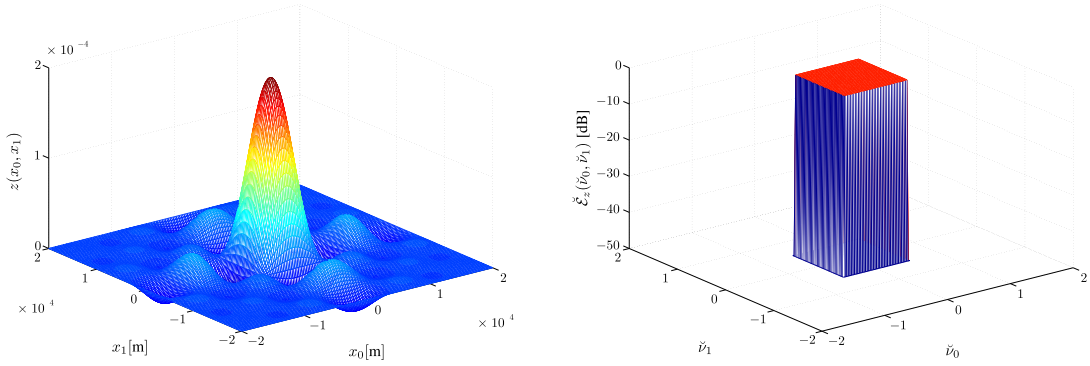

(a) Signal to be reconstructed

(b) Normalized ESD of the signal to be reconstructed

Fig. 1. Example of signal to be reconstructed and its normalized ESD in $\mathbb{R}^2$, respectively described by (2) and (3) with $B_0 = B_1 = B = 10^{-4}$[m^{-1}].

spatial frequency band $\mathcal{B}$ of $z(\mathbf{x})$ as the set of all $\boldsymbol{\nu}$ for which $|Z(\boldsymbol{\nu})|$ is significantly different than zero, $|\mathcal{B}| = |\mathcal{B}_{\mathsf{w}}| + O(\frac{1}{l^d})$ where $l \triangleq \max\{\ell : \mathcal{C}_\ell^{(d)} \subseteq \mathcal{A}\}$ [41]. The signal bandwidth-per-dimension, in the spatial frequency domain, is $B \triangleq \min\{\ell : \mathcal{B} \subseteq \mathcal{C}_\ell^{(d)}\}$. The truncated signal $z(\mathbf{x})$, instantiation of the random process $\mathsf{z}(\mathbf{x}) \triangleq \mathsf{w}(\mathbf{x})\mathbb{1}_{\mathcal{A}}(\mathbf{x})$, is reconstructed by interpolating a numerable set of its samples. The ESD of $z(\mathbf{x})$ is $\mathcal{E}_z(\boldsymbol{\nu}) = \boldsymbol{\mathcal{F}}\{\int_{\mathbb{R}^d} z(\mathbf{x})z^\dagger(\mathbf{x}-\boldsymbol{\tau})d\mathbf{x}\}(\boldsymbol{\nu}) = |Z(\boldsymbol{\nu})|^2$, while that of $\mathsf{z}(\mathbf{x})$ is $\mathcal{E}_{\mathsf{z}}(\boldsymbol{\nu}) = \boldsymbol{\mathcal{F}}\{\int_{\mathbb{R}^d} \mathbb{E}\{\mathsf{z}(\mathbf{x})\mathsf{z}^\dagger(\mathbf{x}-\boldsymbol{\tau})\}d\mathbf{x}\}(\boldsymbol{\nu}) = \mathbb{E}\{|\mathsf{Z}(\boldsymbol{\nu})|^2\}$ with $\mathsf{Z}(\boldsymbol{\nu}) \triangleq \boldsymbol{\mathcal{F}}\{\mathsf{z}(\mathbf{x})\}(\boldsymbol{\nu})$.

Define the normalized spatial coordinate $\breve{\mathbf{x}} \triangleq 2B\mathbf{x}$ and spatial frequency $\breve{\boldsymbol{\nu}} \triangleq \boldsymbol{\nu}/(2B)$. The FT of a normalized signal $\breve{z}(\breve{\mathbf{x}}) \triangleq \frac{1}{\sqrt{E_z}(2B)^{d/2}} z\left(\frac{\breve{\mathbf{x}}}{2B}\right)$ (unitary bandwidth and energy) is

$$\breve{Z}(\breve{\boldsymbol{\nu}}) = \frac{(2B)^{d/2}}{\sqrt{E_z}} Z(2B\breve{\boldsymbol{\nu}}) \tag{1}$$

and the normalized ESD of $z(\mathbf{x})$ is $\breve{\mathcal{E}}_z(\breve{\boldsymbol{\nu}}) \triangleq \frac{(2B)^d}{E_z}\mathcal{E}_z(2B\breve{\boldsymbol{\nu}})$. From (1), $\breve{\mathcal{E}}_z(\breve{\boldsymbol{\nu}}) = \mathcal{E}_{\breve{z}}(\breve{\boldsymbol{\nu}}) = |\breve{Z}(\breve{\boldsymbol{\nu}})|^2$ and $\int_{\mathbb{R}^d}\breve{\mathcal{E}}_z(\breve{\boldsymbol{\nu}})\,d\breve{\boldsymbol{\nu}} = 1$.

Example: Consider the reconstruction of process instantiation (see Fig. 1(a)) expressed by [46][5]

$$z(\mathbf{x}) = \sqrt{E_z}\prod_{i=0}^{d-1}(2B_i)^{\frac{1}{2}}\operatorname{sinc}(2B_i x_i) \tag{2}$$

for which (see Fig. 1(b))

$$\breve{\mathcal{E}}_z(\breve{\boldsymbol{\nu}}) = \prod_{i=0}^{d-1}\frac{1}{2b_i}\operatorname{rect}\left(\frac{\breve{\nu}_i}{2b_i}\right) \tag{3}$$

where $b_i \triangleq B_i/(2B)$ is the normalized bandwidth-per-dimension.

B. Inhomogeneous Sampling Process

Consider a sampling process in which samples are gathered at independent random positions in $\mathbb{R}^d$ according to an inhomogeneous PPP $\boldsymbol{\Pi}$ with intensity $\lambda(\mathbf{x})$ at $\mathbf{x} \in \mathbb{R}^d$[62]. The sampling intensity $\lambda(\mathbf{x})$ is defined so that $\mathbb{E}\{N_\Pi(\mathcal{A})\} = \int_{\mathcal{A}}\lambda(\mathbf{x})\,d\mathbf{x}$ for any $\mathcal{A} \subseteq \mathbb{R}^d$[26], where $N_\Pi(\mathcal{A})$ is the number of points in $\mathcal{A}$

[5]The $\operatorname{sinc}(x) \triangleq \sin(\pi x)/(\pi x)$ for $x \neq 0$ and to 1 for $x = 0$.

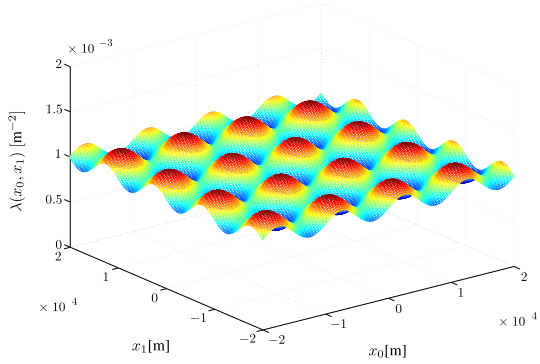

Fig. 2. Example of inhomogeneous PSP intensity in $\mathbb{R}^2$ $(d = 2)$ described by (5) with $\overline{\lambda} = 10^{-3}$[m^{-2}], $a_i = 0.1$, and $B_{\lambda i} = 10^{-4}$[m^{-1}].

(counting measure). The average sampling intensity in $\mathbb{R}^d$ can be written as $\overline{\lambda} = \lim_{\ell\to\infty}\mathbb{E}\left\{N_\Pi(\mathcal{C}_\ell^{(d)})\right\}/|\mathcal{C}_\ell^{(d)}|$.[6] The random sampling process is[7]

$$\mathcal{S}(\mathbf{x}) \triangleq \sum_{n\in\mathcal{N}_\Pi}\delta(\mathbf{x}-\mathbf{x}_n) \tag{4}$$

where $\mathcal{N}_\Pi$ denotes the index set of $\boldsymbol{\Pi}$. The random sampling process has mean $\mu_{\mathcal{S}}(\mathbf{x}) = \mathbb{E}\left\{\sum_{n\in\mathcal{N}_\Pi}\delta(\mathbf{x}-\mathbf{x}_n)\right\}$, with d-dimensional FT $\mathcal{U}_{\mathcal{S}}(\boldsymbol{\nu}) = \mathbb{E}\left\{\sum_{n\in\mathcal{N}_\Pi}e^{-\jmath 2\pi\boldsymbol{\nu}\cdot\mathbf{x}_n}\right\}$, and autocorrelation $R_{\mathcal{S}}(\mathbf{x},\boldsymbol{\tau}) \triangleq \mathbb{E}\{\mathcal{S}(\mathbf{x})\mathcal{S}(\mathbf{x}-\boldsymbol{\tau})\}$.

Example: Consider samples randomly distributed according to an inhomogeneous PSP with intensity $\lambda(\mathbf{x})$ given by (see Fig. 2)

$$\lambda(\mathbf{x}) = \overline{\lambda}\prod_{i=0}^{d-1}[1 + a_i\sin(2\pi B_{\lambda i}x_i)] \tag{5}$$

where $a_i \in [0,1]$ is the inhomogeneity amplitude parameter and $b_{\lambda_i} \triangleq B_{\lambda i}/(2B)$ is the inhomogeneity frequency parameter.

[6]The homogeneous case can be seen as a particular case of the inhomogeneous case with $\lambda(\mathbf{x}) = \overline{\lambda}$, $\forall x \in \mathbb{R}^d$.

[7]The notation based on Dirac delta generalized functions will simplify the analysis of signal reconstruction via interpolation filtering.

C. Sample Loss Model

Consider a set of independent, identically distributed (IID) binomial random variables (RVs) a_n for $n \in \mathcal{N}_{\mathbf{\Pi}}$. Each a_n takes value 1 or 0 when the corresponding n-th sample at x_n is available or unavailable for signal reconstruction, respectively, with probabilities $q_n = q(\mathsf{x}_n) = \mathbb{P}\{\mathsf{a}_n = 1\} = \mathbb{E}\{\mathsf{a}_n\}$ and $p_n = 1 - q_n$. The $q(\mathbf{x})$ has FT $Q(\boldsymbol{\nu})$ and the a_n's are independent of $\mathbf{\Pi}$.[8] The average sample availability is $\overline{q} = \lim_{\ell\to\infty}\mathbb{E}\big\{\frac{1}{N_{\Pi}(\mathcal{C}_\ell^{(d)})}\sum_{n\in\mathcal{N}_\ell} q_n\big\}$ where $\mathcal{N}_\ell$ denotes the index set of $\mathbf{\Pi}\cap\mathcal{C}_\ell^{(d)}$.

The random sampling process with losses, together with its mean and its autocorrelation function, can respectively be written as

$$\mathcal{L}(\mathbf{x}) \triangleq \sum_{n\in\mathcal{N}_{\mathbf{\Pi}}} \mathsf{a}_n \delta(\mathbf{x}-\mathsf{x}_n) \tag{6}$$

with $\mu_{\mathcal{L}}(\mathbf{x}) \triangleq \mathbb{E}\{\mathcal{L}(\mathbf{x})\} = q(\mathbf{x})\mu_{\mathcal{S}}(\mathbf{x})$ and $R_{\mathcal{L}}(\mathbf{x},\boldsymbol{\tau}) \triangleq \mathbb{E}\{\mathcal{L}(\mathbf{x})\mathcal{L}(\mathbf{x}-\boldsymbol{\tau})\}$. The d-dimensional FT of $\mu_{\mathcal{L}}(\mathbf{x})$ is

$$\mathcal{U}_{\mathcal{L}}(\boldsymbol{\nu}) = (Q * \mathcal{U}_{\mathcal{S}})(\boldsymbol{\nu}). \tag{7}$$

D. Sample Position Uncertainties Model

Consider a multidimensional random sampling process with uncertainties in sample positions. In particular, the n-th sample position x_n is imperfectly known as $\widehat{\mathsf{x}}_n$, with a corresponding sample position error $\mathbf{e}_{\mathrm{s}n} \triangleq \widehat{\mathsf{x}}_n - \mathsf{x}_n$ [46]. The estimated position errors $\mathbf{e}_{\mathrm{s}n}$ are zero-mean IID RVs, and independent of a_n and x_n.[9] The characteristic function (CF) of $\mathbf{e}_{\mathrm{s}n}$ is $\Psi_{\mathbf{e}_{\mathrm{s}}}(j\boldsymbol{\nu}) \triangleq \mathbb{E}\{e^{j\boldsymbol{\nu}\cdot\mathbf{e}_{\mathrm{s}}}\}$ and $\Phi_{\mathbf{e}_{\mathrm{s}}}(\boldsymbol{\nu}) \triangleq \boldsymbol{\mathcal{F}}\{f_{\mathbf{e}_{\mathrm{s}}}(\mathbf{e}_{\mathrm{s}})\}(\boldsymbol{\nu}) = \Psi_{\mathbf{e}_{\mathrm{s}}}(-j2\pi\boldsymbol{\nu})$.[10]

The signal sampled with uncertainties (losses and sample position errors) is an instantiation of the process $\mathsf{z}_{\mathrm{u}}(\mathbf{x})$ having FT $\mathsf{Z}_{\mathrm{u}}(\boldsymbol{\nu})$ given by

$$\mathsf{z}_{\mathrm{u}}(\mathbf{x}) \triangleq \sum_{n\in\mathcal{N}_{\mathbf{\Pi}}} \mathsf{a}_n z(\mathsf{x}_n)\,\delta\big(\mathbf{x}-\widehat{\mathsf{x}}_n\big) \tag{8a}$$

$$\mathsf{Z}_{\mathrm{u}}(\boldsymbol{\nu}) = \sum_{n\in\mathcal{N}_{\mathbf{\Pi}}} \mathsf{a}_n z(\mathsf{x}_n)\, e^{-j2\pi\boldsymbol{\nu}\cdot\widehat{\mathsf{x}}_n}. \tag{8b}$$

E. Interpolation Filtering

The reconstruction of $z(\mathbf{x})$ from its samples via LSI filtering is

$$\widehat{\mathsf{z}}(\mathbf{x}) = (\mathsf{z}_{\mathrm{u}} * \theta)(\mathbf{x}) = \sum_{n\in\mathcal{N}_{\mathbf{\Pi}}} \mathsf{a}_n z(\mathsf{x}_n)\,\theta\big(\mathbf{x}-\widehat{\mathsf{x}}_n\big) \tag{9}$$

where $\theta(\mathbf{x}) \in \mathbb{R}$ is the interpolation filtering function with d-dimensional FT $\Theta(\boldsymbol{\nu})$.[11] The d-dimensional band $\mathcal{B}_\theta$ of the interpolator has cardinality[12]

$$|\mathcal{B}_\theta| \triangleq \frac{\int_{\mathbb{R}^d}|\Theta(\boldsymbol{\nu})|^2 d\boldsymbol{\nu}}{|\Theta(\mathbf{0})|^2}. \tag{10}$$

Recall that for regular sampling at Nyquist rate-per-dimension $2B$ the ideal low-pass (ILP) interpolation filtering is commonly employed, i.e., $\Theta(\boldsymbol{\nu}) = \frac{1}{(2B)^d}\mathbb{1}_{\mathcal{B}}(\boldsymbol{\nu})$ thus $|\mathcal{B}_\theta| = |\mathcal{B}| = (2B)^d$.[13] For random sampling in $\mathbb{R}^d$, two oversampling factors are considered

$$\iota_\lambda \triangleq \frac{\overline{\lambda}}{(2B)^d} \tag{11a}$$

$$\iota_{\mathcal{B}_\theta} \triangleq \frac{|\mathcal{B}_\theta|}{(2B)^d} \tag{11b}$$

respectively for the sampling intensity and for the interpolator band.

III. Multidimensional Signal Reconstruction

Theorems for the reconstructed signal spectrum and the signal reconstruction MSE with multidimensional random sampling are provided in the following.

A. Reconstructed Signal Spectrum

The power spectral density (PSD) of a one-dimensional signal reconstructed via random sampling was first studied by Shapiro and Silverman who provided sufficient conditions for alias-free sampling [64]. Then, Beutler and Masry derived expressions for PSD reconstruction through random sampling [65]–[70]. The same kind of problem was also addressed by Parzen in the case of a randomness due sample losses [71]. The aforementioned results are available for stationary point processes in one dimension. We extend them for inhomogeneous (non-stationary) multidimensional random sampling, starting from the next two lemmas.

Lemma 1: Consider a finite-energy signal $y: \mathbb{R}^d \to \mathbb{C}$ sampled with losses according to

$$\mathsf{y}_{\mathcal{L}}(\mathbf{x}) \triangleq y(\mathbf{x})\ \mathcal{L}(\mathbf{x}) \tag{12}$$

and define the functional

$$\Upsilon_{\mathcal{L}}[y] \triangleq \int_{\mathbb{R}^d} |y(\mathbf{x})|^2 \mu_{\mathcal{L}}(\mathbf{x})\, d\mathbf{x}. \tag{13}$$

The ESD of $\mathsf{y}_{\mathcal{L}}(\mathbf{x})$ is found to be[14]

$$\mathcal{E}_{\mathsf{y}_{\mathcal{L}}}(\boldsymbol{\nu}) = \mathbb{E}\Big\{\sum_{n\in\mathcal{N}_{\mathbf{\Pi}}}\sum_{k\in\mathcal{N}_{\mathbf{\Pi}}} \mathsf{a}_n\mathsf{a}_k y(\mathsf{x}_n)\, y^{\dagger}(\mathsf{x}_k)\, e^{-j2\pi\boldsymbol{\nu}\cdot(\mathsf{x}_n-\mathsf{x}_k)}\Big\} \tag{14}$$

and

$$\Upsilon_{\mathcal{L}}[y] = \mathbb{E}\Big\{\sum_{n\in\mathcal{N}_{\mathbf{\Pi}}} q_n |y(\mathsf{x}_n)|^2\Big\}. \tag{15}$$

[8] For example, consider a network of sensors with different energy consumptions leading to different abilities to transmit information to the interpolation entity (the charge of a sensor is independent of that of other sensors).

[9] The probability distribution function (PDF) of the sample position error depends on the technology used to determine the position of the n-th sample in $\mathbb{R}^d$ [63].

[10] The index n is avoided for notational simplicity since the sample position errors are IID.

[11] Hereafter, we will refer to $\Theta(\boldsymbol{\nu})$ as interpolator function.

[12] In one dimension, this cardinality corresponds to twice the effective bandwidth of the interpolator.

[13] It corresponds to $\theta(x) = \mathrm{sinc}(2Bx)$ in one-dimension ($x \in \mathbb{R}$).

[14] The sampled signal $\mathsf{y}_{\mathcal{L}}(\mathbf{x})$ becomes $\mathsf{y}_{\mathcal{S}}(\mathbf{x})$ when $a_n = 1 \forall n \in \mathcal{N}_{\mathbf{\Pi}}$ (i.e., $\mathcal{L} \equiv \mathcal{S}$) with corresponding ESD $\mathcal{E}_{\mathsf{y}_{\mathcal{S}}}(\boldsymbol{\nu})$.

Proof: See Appendix A. □

Lemma 2: Consider a finite-energy signal $y : \mathbb{R}^d \to \mathbb{C}$ sampled without losses according to

$$\mathsf{y}_{\mathcal{S}}(\mathbf{x}) \triangleq y(\mathbf{x})\, \mathcal{S}(\mathbf{x}) \tag{16}$$

and define the functional

$$\Upsilon_{\mathcal{S}}[y] \triangleq \int_{\mathbb{R}^d} |y(\mathbf{x})|^2 \mu_{\mathcal{S}}(\mathbf{x})\, d\mathbf{x}\,. \tag{17}$$

It results

$$\mathcal{U}_{\mathcal{S}}(\boldsymbol{\nu}) = \Lambda(\boldsymbol{\nu}) \tag{18a}$$

$$\mathcal{E}_{\mathsf{y}_{\mathcal{S}}}(\boldsymbol{\nu}) = |(\Lambda * Y)(\boldsymbol{\nu})|^2 + \Upsilon_{\mathcal{S}}[y] \tag{18b}$$

where $\Lambda(\boldsymbol{\nu}) \triangleq \boldsymbol{\mathcal{F}}\{\lambda(\mathbf{x})\}(\boldsymbol{\nu})$, $Y(\boldsymbol{\nu}) \triangleq \boldsymbol{\mathcal{F}}\{y(\mathbf{x})\}(\boldsymbol{\nu})$, and

$$\Upsilon_{\mathcal{S}}[y] = \mathbb{E}\Big\{ \sum_{n \in \mathcal{N}_{\boldsymbol{\Pi}}} y(\mathbf{x}_n)\,|^2 \Big\}. \tag{19}$$

Proof: See Appendix B. □

To determine the ESD of the reconstructed signal, the previous lemmas are applied to the signal $z(\mathbf{x})$.

Lemma 3: The ESD of a signal sampled with losses is found to be

$$\mathcal{E}_{\mathsf{z}_{\mathcal{L}}}(\boldsymbol{\nu}) = \mathcal{E}_{z_{\mathrm{qs}}}(\boldsymbol{\nu}) - \Upsilon_{\mathcal{S}}[z_{\mathrm{q}}] + \Upsilon_{\mathcal{L}}[z] \tag{20}$$

where $\mathcal{E}_{z_{\mathrm{qs}}}(\boldsymbol{\nu})$ is the ESD of $z_{\mathrm{qs}}(\mathbf{x}) \triangleq z_{\mathrm{q}}(\mathbf{x})\, \mathcal{S}(\mathbf{x})$ and $z_{\mathrm{q}}(\mathbf{x}) \triangleq q(\mathbf{x})\, z(\mathbf{x})$.

Proof: See Appendix C. □

Lemma 4: The mean of the FT and the mean of the ESD for the process $\mathsf{z}_{\mathrm{u}}(\mathbf{x})$ are respectively given by

$$\mathcal{U}_{\mathsf{z}_{\mathrm{u}}}(\boldsymbol{\nu}) \triangleq \mathbb{E}\{\mathsf{Z}_{\mathrm{u}}(\boldsymbol{\nu})\} = \Phi_{\mathbf{e}_{\mathrm{s}}}(\boldsymbol{\nu})\,(\mathcal{U}_{\mathcal{L}} * Z)(\boldsymbol{\nu}) \tag{21a}$$

$$\begin{aligned}\mathcal{E}_{\mathsf{z}_{\mathrm{u}}}(\boldsymbol{\nu}) &\triangleq \mathbb{E}\left\{|\mathsf{Z}_{\mathrm{u}}(\boldsymbol{\nu})|^2\right\} \\ &= |\Phi_{\mathbf{e}_{\mathrm{s}}}(\boldsymbol{\nu})|^2 \mathcal{E}_{\mathsf{z}_{\mathcal{L}}}(\boldsymbol{\nu}) + \Upsilon_{\mathcal{L}}[z]\left[1 - |\Phi_{\mathbf{e}_{\mathrm{s}}}(\boldsymbol{\nu})|^2\right].\end{aligned} \tag{21b}$$

Proof: See Appendix D. □

The ESD of the reconstructed signal is now derived.

Theorem 1 (ESD of the Reconstructed Signal): The ESD of the signal $\widehat{\mathsf{z}}(\mathbf{x})$ reconstructed with general interpolation function $\Theta(\boldsymbol{\nu})$ is found to be

$$\begin{aligned}\mathcal{E}_{\widehat{\mathsf{z}}}(\boldsymbol{\nu}) &= |\Theta(\boldsymbol{\nu})|^2 |\Phi_{\mathbf{e}_{\mathrm{s}}}(\boldsymbol{\nu})|^2 |(\Lambda * Q * Z)(\boldsymbol{\nu})|^2 \\ &\quad + |\Theta(\boldsymbol{\nu})|^2 \alpha \overline{\lambda}\, \overline{q}\, E_z\end{aligned} \tag{22}$$

where

$$\alpha \triangleq \frac{\int_{\mathbb{R}^d} \lambda(\mathbf{x})\, q(\mathbf{x})\, |z(\mathbf{x})|^2 d\mathbf{x}}{\overline{\lambda}\, \overline{q}\, E_z}. \tag{23}$$

Proof: Apply Lemmas 1–4 as shown in Appendix E. □

Remark 1: The first term in (22) represents the spectrum of the original signal modified by the effects of random sampling and sample position errors in addition to those of interpolation filtering, while the second term represents an additive noise.

Remark 2: Consider a sampling intensity $\lambda(\mathbf{x})$ and a sample availability $q(\mathbf{x})$ both band-limited with maximum spatial bandwidth-per-dimension B_λ and B_q, respectively.[15] Therefore, $(\Lambda * Q * Z)(\boldsymbol{\nu})$ can be considered extinguished outside $\mathcal{C}_{B_{\mathrm{s}}}$ where $B_{\mathrm{s}} \triangleq B + B_\lambda + B_q$. From Theorem 1, the interpolator band in $\mathbb{R}^d$ has to contain all the spectral components of $(\Lambda * Q * Z)(\boldsymbol{\nu})$ to reconstruct the original signal $z(\mathbf{x})$. Thus, the B_λ and B_q respectively represent the increase per dimension of the Nyquist sampling rate respectively due to the inhomogeneous sampling intensity and the inhomogeneous sample availability.

Remark 3: According to Theorem 1, while the effects of sample position errors over the reconstructed signal ESD can be compensated by a proper interpolator those of the inhomogeneous sampling intensity causes a distortion, due to the convolution $(\Lambda * Q * Z)(\boldsymbol{\nu})$, which cannot be compensated by a realizable linear filtering (as it will be shown in Section IV).

Corollary 1 (Homogeneous PSP With General Interpolator): In case of homogeneous PSP with $\lambda(\mathbf{x}) = \overline{\lambda}$ and homogeneous sample availability with $q(\mathbf{x}) = \overline{q}$, the ESD of the reconstructed signal $\widehat{\mathsf{z}}(\mathbf{x})$ with general interpolation function $\Theta(\boldsymbol{\nu})$ results in

$$\mathcal{E}_{\widehat{\mathsf{z}}}(\boldsymbol{\nu}) = |\Theta(\boldsymbol{\nu})|^2\, \overline{q}^2\, \overline{\lambda}^{-2} |\Phi_{\mathbf{e}_{\mathrm{s}}}(\boldsymbol{\nu})|^2 \mathcal{E}_z(\boldsymbol{\nu}) + |\Theta(\boldsymbol{\nu})|^2 \overline{q}\overline{\lambda} E_z\,. \tag{24}$$

Proof: For $\lambda(\mathbf{x}) = \overline{\lambda}$ and $q(\mathbf{x}) = \overline{q}$, (23) leads to $\alpha = 1$. Thus, (22) reduces to (24) since $\Lambda(\boldsymbol{\nu}) = \overline{\lambda}\delta(\boldsymbol{\nu})$ and $Q(\mathbf{x}) = \overline{q}\delta(\boldsymbol{\nu})$. □

Remark 4: In the absence of sample losses ($\overline{q} = 1$) and of sample position errors ($\Phi_{\mathbf{e}_{\mathrm{s}}}(\boldsymbol{\nu}) = 1$), Corollary 1 reduces to the result of Marvasti [27] after ILP interpolation considering the ESD instead of the PSD.

To highlight the effects of inhomogeneities (in sample distribution and in sample loss), of signal bandwidth-per-dimension, and of sample position errors, the following functions are defined in terms of the normalized spatial frequency. The normalized spatial frequency bands of the signal and of the interpolator function are defined as $\breve{\mathcal{B}} \triangleq \{\breve{\boldsymbol{\nu}}\,\mathrm{s.t.}\, 2B\breve{\boldsymbol{\nu}} \in \mathcal{B}\}$ and $\breve{\mathcal{B}}_\theta \triangleq \{\breve{\boldsymbol{\nu}}\,\mathrm{s.t.}\, 2B\breve{\boldsymbol{\nu}} \in \mathcal{B}_\theta\}$, respectively. The normalized $\Lambda(\boldsymbol{\nu})$ and $Q(\boldsymbol{\nu})$ are

$$\breve{\Lambda}(\breve{\boldsymbol{\nu}}) \triangleq \frac{(2B)^d}{\overline{\lambda}} \Lambda(2B\breve{\boldsymbol{\nu}}) \tag{25a}$$

$$\breve{Q}(\breve{\boldsymbol{\nu}}) \triangleq \frac{(2B)^d}{\overline{q}} Q(2B\breve{\boldsymbol{\nu}})\,. \tag{25b}$$

The standard deviation of the position error normalized to $1/(2B)$, proportional to the signal spatial correlation per dimension, and the normalized function $\breve{\Phi}(\breve{\boldsymbol{\nu}})$ are[16]

$$\breve{\sigma}_{\mathbf{e}_{\mathrm{s}}} \triangleq 2B\, \sigma_{\mathbf{e}_{\mathrm{s}}} \tag{26a}$$

$$\breve{\Phi}(\sigma_{\mathbf{e}_{\mathrm{s}}} \boldsymbol{\nu}) \triangleq \Phi_{\mathbf{e}_{\mathrm{s}}}(\boldsymbol{\nu})\,. \tag{26b}$$

From (26a) and (26b) it follows that $\breve{\Phi}(\breve{\sigma}_{\mathbf{e}_{\mathrm{s}}} \breve{\boldsymbol{\nu}}) = \Phi_{\mathbf{e}_{\mathrm{s}}}(2B\breve{\boldsymbol{\nu}})$. The interpolation function and the interpolator parameter are

[15] The spectra of $\lambda(\mathbf{x})$ and $q(\mathbf{x})$ do not contain significant component outside $\mathcal{C}_{B_\lambda}$ and $\mathcal{C}_{B_q}$, respectively.

[16] Observe that the $\breve{\Phi}(\boldsymbol{\nu})$ in (26b) is equal to the FT of the PDF for the normalized sample position error $\mathbf{e}_{\mathrm{s}}/\sigma_{\mathbf{e}_{\mathrm{s}}}$.

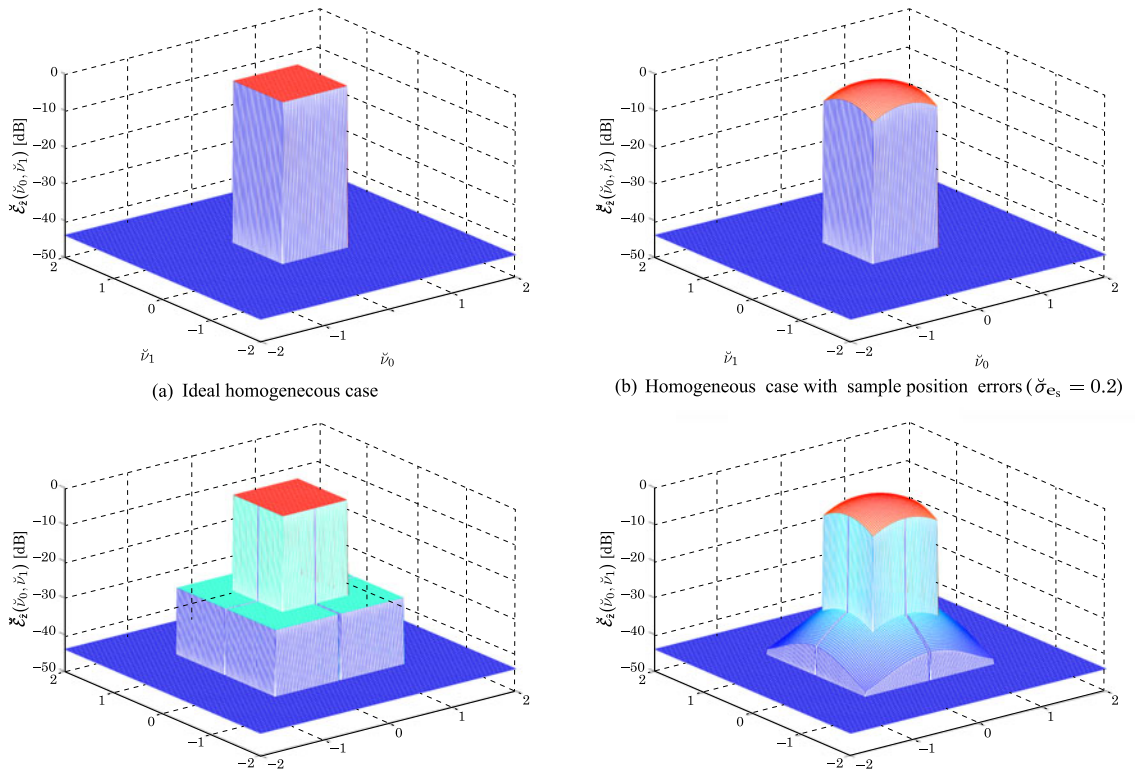

(a) Ideal homogenecous case

(b) Homogeneous case with sample position errors ($\breve{\sigma}_{\mathbf{e}_\mathrm{s}} = 0.2$)

(c) Inhomogeneous case ($\boldsymbol{a}_0 = \boldsymbol{a}_1 = \boldsymbol{a} = 0.1$, $b_{\lambda\,0} = b_{\lambda\,1} = b_\lambda = 0.5$) with sample position errors

(d) Inhomogeneous case ($\boldsymbol{a}_0 = \boldsymbol{a}_1 = \boldsymbol{a} = 0.1$, $b_{\lambda\,0} = b_{\lambda\,1} = b_\lambda = 0.5$) with sample position errors ($\breve{\sigma}_{\mathbf{e}_\mathrm{s}} = 0.2$)

Fig. 3. Example of normalized reconstructed signal ESD in $\mathbb{R}^2$, corresponding to the case of Fig. 1, for $p_n = p = 10^{-3}, \forall n$, $\iota_\lambda = 2.5 \times 10^4$, and $\iota_{\mathcal{B}_\theta} = 25$.

respectively normalized as

$$\breve{\Theta}\left(\frac{\boldsymbol{\nu}}{2B}\right) \triangleq \frac{\Theta(\boldsymbol{\nu})}{\Theta(\mathbf{0})} = \kappa_\theta\, \Theta(\boldsymbol{\nu}) \tag{27a}$$

$$\breve{\kappa}_\theta \triangleq \frac{\kappa_\theta}{(2B)^d}. \tag{27b}$$

The normalized ESD of the reconstructed signal is

$$\breve{\mathcal{E}}_{\widehat{\mathsf{z}}}(\breve{\boldsymbol{\nu}}) \triangleq \frac{(2B)^d}{E_z}\mathcal{E}_{\widehat{\mathsf{z}}}(2B\breve{\boldsymbol{\nu}}). \tag{28}$$

Theorem 2 (Normalized ESD of the Reconstructed Signal): The normalized ESD of the reconstructed signal $\widehat{\mathsf{z}}(\mathbf{x})$ with general normalized interpolation function $\breve{\Theta}(\breve{\boldsymbol{\nu}})$ is found to be

$$\breve{\mathcal{E}}_{\widehat{\mathsf{z}}}(\breve{\boldsymbol{\nu}}) = \overline{q}\,\iota_\lambda \frac{|\breve{\Theta}(\breve{\boldsymbol{\nu}})|^2}{\breve{\kappa}_\theta^2}\left[\overline{q}\,\iota_\lambda \left|\breve{\Phi}\left(\breve{\sigma}_{\mathbf{e}_\mathrm{s}}\breve{\boldsymbol{\nu}}\right)\right|^2 \left|\left(\breve{\Lambda} * \breve{Q} * \breve{Z}\right)(\breve{\boldsymbol{\nu}})\right|^2 + \alpha\right]. \tag{29}$$

Proof: See Appendix F. □

Remark 5: Theorem 2 shows that random sampling and sample position errors affects the signal-to-sampling noise ratio SNR at the interpolator output as

$$\mathsf{SNR} = \frac{\overline{q}\,\iota_\lambda \int_{\mathbb{R}^d} \left|\breve{\Theta}(\breve{\boldsymbol{\nu}})\right|^2 \left|\breve{\Phi}(\breve{\sigma}_{\mathbf{e}_\mathrm{s}}\breve{\boldsymbol{\nu}})\right|^2 \left|\left(\breve{\Lambda} * \breve{Q} * \breve{Z}\right)(\breve{\boldsymbol{\nu}})\right|^2 d\breve{\boldsymbol{\nu}}}{\alpha \int_{\mathbb{R}^d} \left|\breve{\Theta}(\breve{\boldsymbol{\nu}})\right|^2 d\breve{\boldsymbol{\nu}}}.$$

Thus, $\mathsf{SNR} = \frac{\overline{q}\,\iota_\lambda}{\iota_{\mathcal{B}_\theta}} \frac{\beta_\theta}{\alpha}$ that is greater than or equal to 1 iff

$$\overline{q}\overline{\lambda} \geq \alpha \frac{\iota_{\mathcal{B}_\theta}}{\beta_\theta}(2B)^d \tag{30}$$

where β_θ is given by (37b). The factor $\alpha\iota_{\mathcal{B}_\theta}/\beta_\theta$ represents the increasing in the average intensity of available samples with respect to Nyquist rate for obtaining $\mathsf{SNR} \geq 1$(random sampling generates sampling noise) in $\mathbb{R}^d$.[17]

A simple example is now illustrated.

Example: Fig. 3 shows the normalized ESD of the reconstructed signal for the case of Fig. 1 with homogeneous or inhomogeneous PSP in presence or absence of Gaussian distributed sample position errors. According to Theorem 2, it can be observed in Fig. 3(a)–(d) that: (i) the randomness of the sampling process generates itself a background white noise component; (ii) sample position errors cause a spectrum distortion without spectrum enlargement; and (iii) inhomogeneity of the sample process leads to a distortion with spectrum enlargement.

B. Signal Reconstruction MSE

We now analyze the signal reconstruction error for multidimensional inhomogeneous random sampling with sample position uncertainty.

The signal reconstruction MSE is defined as

$$\varepsilon_\mathrm{s} \triangleq \frac{\mathbb{E}\left\{\int_{\mathbb{R}^d} |\widehat{\mathsf{z}}(\mathbf{x}) - z(\mathbf{x})|^2 d\mathbf{x}\right\}}{E_z} \tag{31}$$

[17]This result generalizes the important one in [54] that was obtained for the one-dimensional homogeneous case with ILP interpolator and absence of sample position errors.

which measures the distance between the reconstructed version $\widehat{\mathsf{z}}(\mathbf{x})$ and the original target signal $z(\mathbf{x})$, normalized to its energy.

Theorem 3 (Signal Reconstruction MSE): For an inhomogeneous PSP with intensity $\lambda(\mathbf{x})$, sample availability $q(\mathbf{x})$, and sample position errors with $\Phi_{\mathbf{e}_\mathrm{s}}(\boldsymbol{\nu})$, the signal reconstruction MSE is found to be

$$\varepsilon_\mathrm{s} = \frac{\overline{q}\overline{\lambda}}{\kappa_\theta^2}\left(\alpha\,|\mathcal{B}_\theta| + \beta_\theta\,\overline{q}\overline{\lambda}\right) - \gamma_\theta\,\frac{2\overline{q}\overline{\lambda}}{\kappa_\theta} + 1 \tag{32}$$

where α is given in (23) and

$$\beta_\theta \triangleq \int_{\mathbb{R}^d} |\kappa_\theta\,\Theta(\boldsymbol{\nu})|^2 |\Phi_{\mathbf{e}_\mathrm{s}}(\boldsymbol{\nu})|^2 \frac{|(\Lambda * Q * Z)(\boldsymbol{\nu})|^2}{\overline{\lambda}^2\,\overline{q}^2\,E_z} d\boldsymbol{\nu} \tag{33a}$$

$$\gamma_\theta \triangleq \int_{\mathbb{R}^d} \Re\left\{\kappa_\theta\,\Theta(\boldsymbol{\nu})\,\Phi_{\mathbf{e}_\mathrm{s}}(\boldsymbol{\nu})\,\frac{(\Lambda * Q * Z)(\boldsymbol{\nu})\,Z^\dagger(\boldsymbol{\nu})}{\overline{\lambda}\,\overline{q}\,E_z}\right\} d\boldsymbol{\nu}\,. \tag{33b}$$

Proof: Apply Lemma 4 and Theorem 1 as shown in Appendix G. □

The parameters α, β_θ, and γ_θ of (32) are evaluated in the next section for some cases of interest.

Define two modified ESD as

$$\breve{\mathcal{E}}_{\breve{Z},\breve{Q},\breve{\Lambda},|\breve{\Theta}|^2}(\breve{\boldsymbol{\nu}}) \triangleq |\breve{\Theta}(\breve{\boldsymbol{\nu}})|^2 \left|\left(\breve{\Lambda} * \breve{Q} * \breve{Z}\right)(\breve{\boldsymbol{\nu}})\right|^2 \tag{34a}$$

$$\breve{\mathcal{E}}_{\breve{Z},\breve{Q},\breve{\Lambda},\breve{\Theta}}(\breve{\boldsymbol{\nu}}) \triangleq \Re\left\{\breve{\Theta}(\breve{\boldsymbol{\nu}})\left(\breve{\Lambda} * \breve{Q} * \breve{Z}\right)(\breve{\boldsymbol{\nu}})\,\breve{Z}^\dagger(\breve{\boldsymbol{\nu}})\right\} \tag{34b}$$

which, in the case of homogeneous PSP and homogeneous sample availability, are proportional to the signal ESD when an ILP interpolator filter is used. Remember that, given a continuous function $\varphi(\boldsymbol{\nu})$ with $\varphi(\mathbf{0}) = 1$ and a norm-integrable function $f(\boldsymbol{\nu})$, the φ-mean of $f(\boldsymbol{\nu})$ for any $\sigma \in \mathbb{R}$ is [72]

$$\boldsymbol{\mathcal{M}}_{\sigma,\varphi}\{f(\boldsymbol{\nu})\} \triangleq \int_{\mathbb{R}^d} \varphi(\sigma\boldsymbol{\nu})\,f(\boldsymbol{\nu})\,d\boldsymbol{\nu}. \tag{35}$$

Theorem 4 (Signal Reconstruction MSE with Normalized Quantities): Under the same assumptions of Theorem 3, the signal reconstruction MSE with normalized quantities is found to be

$$\varepsilon_\mathrm{s} = \frac{\overline{q}\iota_\lambda}{\breve{\kappa}_\theta^2}\left(\alpha\,\iota_{\mathcal{B}_\theta} + \beta_\theta\,\overline{q}\iota_\lambda\right) - \gamma_\theta\,\frac{2\overline{q}\iota_\lambda}{\breve{\kappa}_\theta} + 1 \tag{36}$$

with

$$\alpha = \boldsymbol{\mathcal{M}}_{1,\breve{Z}^\dagger * \breve{Z}_-}\left\{\left(\breve{\Lambda} * \breve{Q}\right)(\breve{\boldsymbol{\nu}})\right\} \tag{37a}$$

$$\beta_\theta = \boldsymbol{\mathcal{M}}_{\breve{\sigma}_{\mathbf{e}_\mathrm{s}},|\breve{\Phi}|^2}\left\{\breve{\mathcal{E}}_{\breve{Z},\breve{Q},\breve{\Lambda},|\breve{\Theta}|^2}(\breve{\boldsymbol{\nu}})\right\} \tag{37b}$$

$$\gamma_\theta = \boldsymbol{\mathcal{M}}_{\breve{\sigma}_{\mathbf{e}_\mathrm{s}},\breve{\Phi}}\left\{\breve{\mathcal{E}}_{\breve{Z},\breve{Q},\breve{\Lambda},\breve{\Theta}}(\breve{\boldsymbol{\nu}})\right\} \tag{37c}$$

where $\breve{Z}_-(\breve{\boldsymbol{\nu}}) \triangleq \breve{Z}(-\breve{\boldsymbol{\nu}})$.

Proof: See Appendix H. □

Note that the sample position errors affect the parameters β_θ and γ_θ only, while they do not affect α.

Hereafter, Theorem 4 is used to determine novel results on the signal reconstruction MSE for some cases of interest on the sample position errors.

Corollary 2 (Gaussian Distributed Sample Position Errors): For zero-mean Gaussian IID sample position errors with normalized variance $\breve{\sigma}_{\mathbf{e}_\mathrm{s}}^2$, general interpolator, inhomogeneous PSP with intensity $\lambda(\mathbf{x})$, and sample availability $q(\mathbf{x})$, the signal reconstruction MSE is given by (36) with α as in (37a) and

$$\beta_\theta = \left(4\pi\,t_{\breve{\sigma}_{\mathbf{e}_\mathrm{s}}}\right)^{\frac{d}{2}} \boldsymbol{\mathcal{W}}_{t_{\breve{\sigma}_{\mathbf{e}_\mathrm{s}}}}\left\{\breve{\mathcal{E}}_{\breve{Z},\breve{Q},\breve{\Lambda},|\breve{\Theta}|^2}(\breve{\boldsymbol{\nu}})\right\}(\mathbf{0}) \tag{38a}$$

$$\gamma_\theta = \left(8\pi\,t_{\breve{\sigma}_{\mathbf{e}_\mathrm{s}}}\right)^{\frac{d}{2}} \boldsymbol{\mathcal{W}}_{2t_{\breve{\sigma}_{\mathbf{e}_\mathrm{s}}}}\left\{\breve{\mathcal{E}}_{\breve{Z},\breve{Q},\breve{\Lambda},\breve{\Theta}}(\breve{\boldsymbol{\nu}})\right\}(\mathbf{0}) \tag{38b}$$

where $t_{\breve{\sigma}_{\mathbf{e}_\mathrm{s}}} \triangleq \left(4\pi\,\breve{\sigma}_{\mathbf{e}_\mathrm{s}}\right)^{-2}$ and

$$\boldsymbol{\mathcal{W}}_t\{f(\boldsymbol{\nu})\}(\mathbf{x}) \triangleq \frac{1}{(4\pi\,t)^{\frac{d}{2}}}\int_{\mathbb{R}^d} f(\boldsymbol{\nu})\,e^{-\frac{\|\mathbf{x}-\boldsymbol{\nu}\|^2}{4t}} d\boldsymbol{\nu}. \tag{39}$$

is the Weierstrass transform [73] with parameter t for $f(\boldsymbol{\nu})$ in $\mathbb{R}^d$, where $\|\cdot\|$ denotes the Euclidean norm.

Proof: From (26b), the Gaussian hypothesis on $\mathbf{e}_\mathrm{s}$ gives $\breve{\Phi}(\breve{\sigma}_{\mathbf{e}_\mathrm{s}}\breve{\boldsymbol{\nu}}) = e^{-2\pi^2\|\breve{\sigma}_{\mathbf{e}_\mathrm{s}}\breve{\boldsymbol{\nu}}\|^2}$. Thus, from (39), expressions (37b) and (37c) result in (38a) and (38b), respectively. □

Corollary 3 (Absence of Sample Position Errors): In the absence of sample position errors, general interpolator, inhomogeneous PSP with intensity $\lambda(\mathbf{x})$, and sample availability $q(\mathbf{x})$, the signal reconstruction MSE results in (36) with α as in (37a) and

$$\beta_\theta = \int_{\mathbb{R}^d} \breve{\mathcal{E}}_{\breve{Z},\breve{Q},\breve{\Lambda},|\breve{\Theta}|^2}(\breve{\boldsymbol{\nu}})\,d\breve{\boldsymbol{\nu}} = \boldsymbol{\mathcal{F}}^{-1}\left\{\breve{\mathcal{E}}_{\breve{Z},\breve{Q},\breve{\Lambda},|\breve{\Theta}|^2}(\breve{\boldsymbol{\nu}})\right\}(\mathbf{0}) \tag{40a}$$

$$\gamma_\theta = \int_{\mathbb{R}^d} \breve{\mathcal{E}}_{\breve{Z},\breve{Q},\breve{\Lambda},\breve{\Theta}}(\breve{\boldsymbol{\nu}})\,d\breve{\boldsymbol{\nu}} = \boldsymbol{\mathcal{F}}^{-1}\left\{\breve{\mathcal{E}}_{\breve{Z},\breve{Q},\breve{\Lambda},\breve{\Theta}}(\breve{\boldsymbol{\nu}})\right\}(\mathbf{0})\,. \tag{40b}$$

Proof: In an absence of sample position errors, we have $f_{\mathbf{e}_\mathrm{s}}(\mathbf{e}_\mathrm{s}) = \delta(\mathbf{e}_\mathrm{s})$ and $\Phi_{\mathbf{e}_\mathrm{s}}(\boldsymbol{\nu}) = 1$, therefore (26b) leads to $\breve{\Phi}(\breve{\boldsymbol{\nu}}) = 1$. Thus, (37b) and (37c) lead to (40a) and (40b), respectively. □

To better understand the effects of sample position errors on the signal reconstruction MSE, consider the following two limit cases.

Corollary 4 (Small Sample Position Errors With Respect to Signal Spatial Correlation): Consider an inhomogeneous PSP with intensity $\lambda(\mathbf{x})$ and sample availability $q(\mathbf{x})$. For $\sigma_{\mathbf{e}_\mathrm{s}} \ll 1/(2B)$ the signal reconstruction MSE results in (36) with parameters α, β_θ, γ_θ as for Corollary 3 (absence of sample position errors).

Proof: Since $\lim_{\sigma\to 0}\boldsymbol{\mathcal{M}}_{\sigma,\varphi}\{f(\boldsymbol{\nu})\} = \int_{\mathbb{R}^d} f(\boldsymbol{\nu})\,d\boldsymbol{\nu}$ for any $f : \mathbb{R}^d \to \mathbb{C}$ [72], (37b) and (37c) reduce to (40a) and (40b), respectively. □

Corollary 5 (Large Sample Position Errors with Respect to Signal Spatial Correlation): Consider an inhomogeneous PSP with intensity $\lambda(\mathbf{x})$ and sample availability $q(\mathbf{x})$. For $\sigma_{\mathbf{e}_\mathrm{s}} \gg 1/(2B)$ the signal reconstruction MSE results in

$$\varepsilon_\mathrm{s} = \alpha\,\frac{\overline{q}\iota_\lambda}{\breve{\kappa}_\theta^2}\,\iota_{\mathcal{B}_\theta} + 1\,. \tag{41}$$

Proof: Since $\breve{\Phi}$ is the FT of a PDF, $\breve{\Phi}(\sigma\breve{\boldsymbol{\nu}})$ and $|\breve{\Phi}(\sigma\breve{\boldsymbol{\nu}})|^2$ tend to 0 for σ approaching infinity. Thus (37b) and (37c) tend to 0 for $\breve{\sigma}_{\mathbf{e}_\mathrm{s}}$ approaching infinity, and from Theorem 4 with $\beta_\theta = \gamma_\theta = 0$ we obtain (41). □

Remark 6: Corollaries 4 and 5 indicate that the impact of sample position errors on the signal reconstruction MSE does not depend on the value of position error variance itself, but rather on its normalized value with respect to the spatial correlation of the signal. The higher is the spatial correlation of the signal, the more negligible results the additive MSE due to sample position errors up to the point where Corollary 3 holds.

Corollary 6 (Homogeneous PSP): Consider a homogeneous PSP with intensity $\lambda(\mathbf{x}) = \overline{\lambda}$, sample availability $q(\mathbf{x}) = \overline{q}$, and presence of sample position errors. The signal reconstruction MSE for a general interpolator results in (36) with

$$\alpha = 1 \tag{42a}$$

$$\beta_\theta = \boldsymbol{\mathcal{M}}_{\breve{\sigma}_{\mathbf{e}_\mathrm{s}},|\breve{\Phi}|^2}\left\{|\breve{\Theta}(\breve{\boldsymbol{\nu}})|^2\,\breve{\mathcal{E}}_z(\breve{\boldsymbol{\nu}})\right\} \tag{42b}$$

$$\gamma_\theta = \boldsymbol{\mathcal{M}}_{\breve{\sigma}_{\mathbf{e}_\mathrm{s}},\breve{\Phi}}\left\{\Re\left\{\breve{\Theta}(\breve{\boldsymbol{\nu}})\right\}\breve{\mathcal{E}}_z(\breve{\boldsymbol{\nu}})\right\}. \tag{42c}$$

Proof: By substituting the FT of $\lambda(\mathbf{x}) = \overline{\lambda}$ and $q(\mathbf{x}) = \overline{q}$ in (25a) and (25b), respectively, we obtain

$$\breve{\Lambda}(\breve{\boldsymbol{\nu}}) = (2B)^d\delta(2B\breve{\boldsymbol{\nu}}) = \delta(\breve{\boldsymbol{\nu}}) \tag{43a}$$

$$\breve{Q}(\breve{\boldsymbol{\nu}}) = (2B)^d\delta(2B\breve{\boldsymbol{\nu}}) = \delta(\breve{\boldsymbol{\nu}}) \tag{43b}$$

in the sense of distributions. Thus, from (37a) α results in

$$\alpha = \boldsymbol{\mathcal{M}}_{1,\breve{Z}^\dagger*\breve{Z}_-}[\delta] = \left(\breve{Z}*\breve{Z}_-^\dagger\right)(\mathbf{0}) = \int_{\mathbb{R}^d}|\breve{Z}(\breve{\boldsymbol{\nu}})|^2 d\breve{\boldsymbol{\nu}} = 1.$$

Also, (34b) and (34a) lead to

$$\breve{\mathcal{E}}_{\breve{Z},\breve{Q},\breve{\Lambda},\breve{\Theta}}(\breve{\boldsymbol{\nu}}) = \Re\left\{\breve{\Theta}(\breve{\boldsymbol{\nu}})\right\}\breve{\mathcal{E}}_z(\breve{\boldsymbol{\nu}})$$

$$\breve{\mathcal{E}}_{\breve{Z},\breve{Q},\breve{\Lambda},|\breve{\Theta}|^2}(\breve{\boldsymbol{\nu}}) = |\breve{\Theta}(\breve{\boldsymbol{\nu}})|^2\breve{\mathcal{E}}_z(\breve{\boldsymbol{\nu}})$$

which gives (42b) and (42c) from (37b) and (37c). □

Remark 7: Corollary 6 shows that the effect of sample position errors is present in β_θ and γ_θ jointly with $\breve{\Theta}(\breve{\boldsymbol{\nu}})$. Therefore, it can be mitigated by a proper interpolation filtering.

IV. Interpolation Filtering

The impact of the interpolation filter on the signal reconstruction MSE is now analyzed.

A. ILP Interpolator

Recent works related to sensor networks consider an ILP interpolation filter[18] in the form of

$$\Theta(\boldsymbol{\nu}) = \frac{1}{\kappa_\theta}\mathbb{1}_{\mathcal{B}_\theta}(\boldsymbol{\nu}) \tag{45}$$

without accounting for inhomogeneous PSP and sample position errors [75].

Corollary 7 (ILP Interpolator): In the setting of Theorem 4, for ILP interpolator $\breve{\Theta}(\breve{\boldsymbol{\nu}}) = \mathbb{1}_{\breve{\mathcal{B}}_\theta}(\breve{\boldsymbol{\nu}})$ with $\breve{\mathcal{B}}_\mathrm{s} \subseteq \breve{\mathcal{B}}_\theta$, where $\breve{\mathcal{B}}_\mathrm{s} \triangleq \{\breve{\boldsymbol{\nu}}\,\mathrm{s.t.}\,2B\breve{\boldsymbol{\nu}} \in \mathcal{C}_{B_\mathrm{s}}\}$, the signal reconstruction MSE results in (36) with α as in (37a) and

$$\beta_\theta = \boldsymbol{\mathcal{M}}_{\breve{\sigma}_{\mathbf{e}_\mathrm{s}},|\breve{\Phi}|^2}\left\{|\left(\breve{\Lambda}*\breve{Q}*\breve{Z}\right)(\breve{\boldsymbol{\nu}})|^2\right\} \tag{46a}$$

$$\gamma_\theta = \boldsymbol{\mathcal{M}}_{\breve{\sigma}_{\mathbf{e}_\mathrm{s}},\breve{\Phi}}\left\{\Re\left\{\left(\breve{\Lambda}*\breve{Q}*\breve{Z}\right)(\breve{\boldsymbol{\nu}})\,\breve{Z}^\dagger(\breve{\boldsymbol{\nu}})\right\}\right\}. \tag{46b}$$

These reduce, for zero-mean Gaussian IID sample position errors with normalized variance $\breve{\sigma}^2_{\mathbf{e}_\mathrm{s}}$, to

$$\beta_\theta = \left(4\pi\, t_{\breve{\sigma}_{\mathbf{e}_\mathrm{s}}}\right)^{\frac{d}{2}}\boldsymbol{\mathcal{W}}_{t_{\breve{\sigma}_{\mathbf{e}_\mathrm{s}}}}\left\{|\left(\breve{\Lambda}*\breve{Q}*\breve{Z}\right)(\breve{\boldsymbol{\nu}})|^2\right\}(\mathbf{0}) \tag{47a}$$

$$\gamma_\theta = \left(8\pi\, t_{\breve{\sigma}_{\mathbf{e}_\mathrm{s}}}\right)^{\frac{d}{2}}\boldsymbol{\mathcal{W}}_{2t_{\breve{\sigma}_{\mathbf{e}_\mathrm{s}}}}\left\{\Re\left\{\left(\breve{\Lambda}*\breve{Q}*\breve{Z}\right)(\breve{\boldsymbol{\nu}})\,\breve{Z}^\dagger(\breve{\boldsymbol{\nu}})\right\}\right\}(\mathbf{0}). \tag{47b}$$

In the absence of sample position errors

$$\beta_\theta = \int_{\mathbb{R}^d}\breve{\lambda}^2(\breve{\mathbf{x}})\,\breve{q}^2(\breve{\mathbf{x}})\,|\breve{z}(\breve{\mathbf{x}})|^2 d\breve{\mathbf{x}} \tag{48a}$$

$$\gamma_\theta = \int_{\mathbb{R}^d}\breve{\lambda}(\breve{\mathbf{x}})\,\breve{q}(\breve{\mathbf{x}})\,|\breve{z}(\breve{\mathbf{x}})|^2 d\breve{\mathbf{x}} = \alpha \tag{48b}$$

where $\breve{z}(\breve{\mathbf{x}})$, $\breve{\lambda}(\breve{\mathbf{x}})$, and $\breve{q}(\breve{\mathbf{x}})$ are respectively the inverse FTs of $\breve{Z}(\breve{\boldsymbol{\nu}})$, $\breve{\Lambda}(\breve{\boldsymbol{\nu}})$, and $\breve{Q}(\breve{\boldsymbol{\nu}})$.

Proof: Since $z(\mathbf{x})$ is band-limitated, from (1), (25a), and (25b) it follows that $(\breve{\Lambda}*\breve{Q}*\breve{Z})(\breve{\boldsymbol{\nu}})$ does not have spectral components outside $\breve{\mathcal{B}}_\mathrm{s}$. From Theorem 4, by substituting $\breve{\Theta}(\breve{\boldsymbol{\nu}}) = \mathbb{1}_{\breve{\mathcal{B}}_\theta}(\breve{\boldsymbol{\nu}})$ in (34a) and (34b), we obtain (46a) and (46b). In addition, (47a) and (47b) follow from Corollary 2, (34a), and (34b). From (37a), (46a), and (46b) using $\breve{\Phi}(\breve{\boldsymbol{\nu}}) = 1$ and Parseval relation, we obtain (48a) and (48b). □

Corollary 8 (ILP Interpolator—Homogeneous PSP): In the setting of Corollary 6, for ILP interpolator $\breve{\Theta}(\breve{\boldsymbol{\nu}}) = \mathbb{1}_{\breve{\mathcal{B}}_\theta}(\breve{\boldsymbol{\nu}})$ with $\breve{\mathcal{B}} \subseteq \breve{\mathcal{B}}_\theta$, the signal reconstruction MSE results in (36) with $\alpha = 1$ and

$$\beta_\theta = \boldsymbol{\mathcal{M}}_{\breve{\sigma}_{\mathbf{e}_\mathrm{s}},|\breve{\Phi}|^2}\left\{\breve{\mathcal{E}}_z(\breve{\boldsymbol{\nu}})\right\} \tag{49a}$$

$$\gamma_\theta = \boldsymbol{\mathcal{M}}_{\breve{\sigma}_{\mathbf{e}_\mathrm{s}},\breve{\Phi}}\left\{\breve{\mathcal{E}}_z(\breve{\boldsymbol{\nu}})\right\}. \tag{49b}$$

These reduce, for zero-mean Gaussian IID sample position errors with normalized variance $\breve{\sigma}^2_{\mathbf{e}_\mathrm{s}}$, to

$$\beta_\theta = \left(4\pi\, t_{\breve{\sigma}_{\mathbf{e}_\mathrm{s}}}\right)^{\frac{d}{2}}\boldsymbol{\mathcal{W}}_{t_{\breve{\sigma}_{\mathbf{e}_\mathrm{s}}}}\left\{\breve{\mathcal{E}}_z(\breve{\boldsymbol{\nu}})\right\}(\mathbf{0}) \tag{50a}$$

$$\gamma_\theta = \left(8\pi\, t_{\breve{\sigma}_{\mathbf{e}_\mathrm{s}}}\right)^{\frac{d}{2}}\boldsymbol{\mathcal{W}}_{2t_{\breve{\sigma}_{\mathbf{e}_\mathrm{s}}}}\left\{\breve{\mathcal{E}}_z(\breve{\boldsymbol{\nu}})\right\}(\mathbf{0}). \tag{50b}$$

In the absence of sample position errors $\beta_\theta = \gamma_\theta = 1$.

Proof: Apply (43a) and (43b) to results of Corollary 7. □

Remark 8: From Corollary 8 with absence of sample position errors the signal reconstruction MSE reduces to

$$\varepsilon_\mathrm{s} = \frac{\overline{q}\overline{\lambda}}{\kappa_\theta^2}\left(|\mathcal{B}_\theta| + \overline{q}\overline{\lambda}\right) - \frac{2\overline{q}\overline{\lambda}}{\kappa_\theta} + 1. \tag{51}$$

Therefore, results in [41] and [45] can be seen as particular cases of Theorem 3.

To quantify how the knowledge of samples intensity and availability can improve the signal reconstruction, we determine the signal reconstruction MSE for various interpolator parameter κ_θ in (45) designed according to such knowledge. The optimal

[18] Numerical aspects related to practical implementations of such interpolator are addressed in [74].

value of κ_θ minimizing the signal reconstruction MSE is obtained by setting to zero the derivative of (32) with respect to κ_θ, which results in

$$\kappa_\theta = \left(\hat{\alpha}\,|\mathcal{B}_\theta| + \hat{\beta}_\theta\,\overline{q}\overline{\lambda}\right)/\hat{\gamma}_\theta \tag{52}$$

with $\hat{\alpha} = \alpha$, $\hat{\beta}_\theta = \beta_\theta$, and $\hat{\gamma}_\theta = \gamma_\theta$. Thus, (52) depends on parameters α, β_θ, γ_θ, whose expressions (37a), (46a), (46b) require the prior knowledge of the signal to be reconstructed for inhomogeneous PSP. Therefore, three suboptimal cases are considered in addition to the optimal one. In particular, κ_θ is chosen equal the interpolator parameter optimal for the case of homogeneous sampling and in the absence of sample position errors (i.e., from Corollary 8 it is $\hat{\alpha} = \hat{\beta}_\theta = \hat{\gamma}_\theta = 1$, independently of the signal spectrum). The optimal κ_θ is considered as a theoretical benchmark for ILP filtering.

Case 1 (Knowledge of Average Samples' Density): The sample availability is unknown thus assume $\overline{q} = 1$. The unknown interpolator spatial bandwidth $|\mathcal{B}_\theta|$ (related to that of the signal) is considered negligible with respect to $\overline{\lambda}$. Therefore, (52) with $\hat{\alpha} = \hat{\beta}_\theta = \hat{\gamma}_\theta = 1$ provides $\kappa_\theta = \overline{\lambda}$ and (32) results in

$$\varepsilon_{\mathrm{s}} = \alpha\,\frac{\overline{q}}{\overline{\lambda}}|\mathcal{B}_\theta| + \beta_\theta\,\overline{q}^2 - \gamma_\theta\,2\overline{q} + 1. \tag{53}$$

Case 2 (Knowledge of Average Samples' Density and of Sample Loss Probability): The unknown interpolator spatial bandwidth $|\mathcal{B}_\theta|$ is considered negligible with respect to $\overline{q}\overline{\lambda}$. Therefore, (52) with $\hat{\alpha} = \hat{\beta}_\theta = \hat{\gamma}_\theta = 1$ provides $\kappa_\theta = \overline{q}\overline{\lambda}$ and (32) results in

$$\varepsilon_{\mathrm{s}} = \alpha\,\frac{|\mathcal{B}_\theta|}{\overline{q}\overline{\lambda}} + \beta_\theta - 2\gamma_\theta + 1. \tag{54}$$

Case 3 (Knowledge of Average Samples' Density, Loss Probability, and of Signal Spatial Frequency Band): In this case (52) for $\hat{\alpha} = \hat{\beta}_\theta = \hat{\gamma}_\theta = 1$ provides

$$\kappa_\theta = |\mathcal{B}_\theta| + \overline{q}\overline{\lambda} \tag{55}$$

and

$$\varepsilon_{\mathrm{s}} = \frac{q\overline{\lambda}\left(\alpha|\mathcal{B}_\theta| + \beta_\theta\,\overline{q}\overline{\lambda}\right)}{\left(|\mathcal{B}_\theta| + \overline{q}\overline{\lambda}\right)^2} - \frac{2\overline{q}\overline{\lambda}\,\gamma_\theta}{|\mathcal{B}_\theta| + \overline{q}\overline{\lambda}} + 1. \tag{56}$$

Note that Cases 1–3, for $\alpha = \beta_\theta = \gamma_\theta = 1$ (homogeneous PSP without sample position errors), result in subcases presented in [41].

Case 4 (Full Knowledge): Substituting (52) with $\hat{\alpha} = \alpha$, $\hat{\beta}_\theta = \beta_\theta$, and $\hat{\gamma}_\theta = \gamma_\theta$ in (32) gives

$$\varepsilon_{\mathrm{s}} = \frac{\alpha\,|\mathcal{B}_\theta| + \left(\beta_\theta - \gamma_\theta^2\right)\overline{q}\overline{\lambda}}{\alpha\,|\mathcal{B}_\theta| + \beta_\theta\,\overline{q}\overline{\lambda}}. \tag{57}$$

Note that Case 4 reduces to Case 3 for homogeneous PSP without sample position errors.

B. Optimal LSI Interpolator

The optimal interpolation filtering function $\Theta(\boldsymbol{\nu})$ is known only for some specific cases in one dimension [76]. Here, by extending the Wiener filtering theory to the inhomogeneous (thus non-stationary) multidimensional case, we find the optimal LSI interpolator function.

Theorem 5 (Optimal LSI Interpolator for Inhomogeneous PSP): The optimal linear space-invariant interpolator is

$$\Theta(\boldsymbol{\nu}) = \frac{\left[\Phi_{\mathbf{e}_{\mathrm{s}}}(\boldsymbol{\nu})\,(\Lambda * Q * Z)(\boldsymbol{\nu})\right]^\dagger Z(\boldsymbol{\nu})}{|\Phi_{\mathbf{e}_{\mathrm{s}}}(\boldsymbol{\nu})|^2\,|(\Lambda * Q * Z)(\boldsymbol{\nu})|^2 + \alpha\overline{q}\overline{\lambda}E_z} \tag{58}$$

with parameter κ_θ in (81) and equivalent bandwidth in (82).

Proof: See Appendix I. □

Corollary 9 (Optimal LSI for Homogeneous PSP): For homogeneous PSP with intensity $\lambda(\mathbf{x}) = \overline{\lambda}$ and sample availability $q(\mathbf{x}) = \overline{q}$, the optimal LSI interpolator results in

$$\Theta(\boldsymbol{\nu}) = \frac{\Phi^\dagger_{\mathbf{e}_{\mathrm{s}}}(\boldsymbol{\nu})\,\mathcal{E}_z(\boldsymbol{\nu})}{\overline{q}\overline{\lambda}|\Phi_{\mathbf{e}_{\mathrm{s}}}(\boldsymbol{\nu})|^2\mathcal{E}_z(\boldsymbol{\nu}) + E_z}\,. \tag{59}$$

Proof: It follows from (58) with $\alpha = 1$, $Q(\boldsymbol{\nu}) = \overline{q}\delta(\boldsymbol{\nu})$, and $\Lambda(\boldsymbol{\nu}) = \overline{\lambda}\delta(\boldsymbol{\nu})$. □

Remark 9: By comparing the optimal LSI expressions (58) and (59), it can be noticed that inhomogeneity would require prior knowledge of the signal to be reconstructed, while for homogeneous PSP the optimal LSI interpolator requires the knowledge of the ESD only. This makes the LSI optimization mainly useful for deriving theoretical bounds.

In the absence of sample position errors ($\Phi_{\mathbf{e}_{\mathrm{s}}}(\boldsymbol{\nu}) = 1$), the optimal LSI interpolator expression (59) reduces to $\Theta(\boldsymbol{\nu}) = \mathcal{E}_z(\boldsymbol{\nu})\,/\left[\overline{q}\overline{\lambda}\mathcal{E}_z(\boldsymbol{\nu}) + E_z\right]$, which, if the ESD is replaced by a power spectral density, corresponds to the multidimensional extension of the optimal linear time invariant filter for the reconstruction of finite-power signal through a stationary Poisson sampling process as presented in one dimension in [77]–[79].

Theorem 6 (Signal Reconstruction MSE for Optimal LSI Interpolator): For the optimal LSI interpolator (58), the signal reconstruction MSE results in

$$\varepsilon_{\mathrm{s}} = 1 - \frac{1}{E_z}\int_{\mathbb{R}^d}\frac{|\Phi_{\mathbf{e}_{\mathrm{s}}}(\boldsymbol{\nu})|^2\,|(\Lambda * Q * Z)(\boldsymbol{\nu})|^2|Z(\boldsymbol{\nu})|^2}{|\Phi_{\mathbf{e}_{\mathrm{s}}}(\boldsymbol{\nu})|^2\,|(\Lambda * Q * Z)(\boldsymbol{\nu})|^2 + \alpha\overline{q}\overline{\lambda}E_z}d\boldsymbol{\nu}\,. \tag{60}$$

Proof: See Appendix J. □

Corollary 10 (Signal Reconstruction MSE with Optimal LSI Interpolator for Homogeneous PSP): For homogeneous PSP with intensity $\lambda(\mathbf{x}) = \overline{\lambda}$ and sample availability $q(\mathbf{x}) = \overline{q}$, the optimal LSI interpolator (59) provides the signal reconstruction MSE

$$\varepsilon_{\mathrm{s}} = 1 - \frac{1}{E_z}\int_{\mathbb{R}^d}\frac{|\Phi_{\mathbf{e}_{\mathrm{s}}}(\boldsymbol{\nu})|^2\mathcal{E}_z^2(\boldsymbol{\nu})}{|\Phi_{\mathbf{e}_{\mathrm{s}}}(\boldsymbol{\nu})|^2\mathcal{E}_z(\boldsymbol{\nu}) + \frac{E_z}{\overline{q}\overline{\lambda}}}d\boldsymbol{\nu}. \tag{61}$$

Proof: It follows from (60) with $\alpha = 1$, $Q(\boldsymbol{\nu}) = \overline{q}\delta(\boldsymbol{\nu})$, and $\Lambda(\boldsymbol{\nu}) = \overline{\lambda}\delta(\boldsymbol{\nu})$. □

In the absence of sample position errors ($\Phi_{\mathbf{e}_{\mathrm{s}}}(\boldsymbol{\nu}) = 1$), (61) reduces to $\varepsilon_{\mathrm{s}} = \int_{\mathbb{R}^d}\frac{\mathcal{E}_z(\boldsymbol{\nu})}{\overline{q}\overline{\lambda}\mathcal{E}_z(\boldsymbol{\nu}) + E_z}d\boldsymbol{\nu}$, which corresponds to the multidimensional extension of the signal reconstruction presented in one dimension in [77]–[79].

C. Asymptotic Analysis

To provide more insights on what affects the most the signal reconstruction MSE, we study its asymptotic behaviour for a sample intensity large with respect to $(2B)^d$ considering all the aforementioned interpolation techniques.

Corollary 11 (Asymptotic Expression for Signal Reconstruction MSE): For $\iota_\lambda \to \infty$, the asymptotic expression for signal

TABLE II
RECONSTRUCTION MSE FOR $1/\iota_\lambda \to 0$: (A) INHOMOGENEOUS PSP; (B) HOMOGENEOUS PSP; AND (C) HOMOGENEOUS PSP WITHOUT SAMPLE POSITION ERRORS

Interpol.	PSP	floor (c_0)	1st order term (c_1)
ILP	(A)	$\beta_\theta\,\overline{q}^2 - 2\gamma_\theta\,\overline{q} + 1$	$\alpha\overline{q}\iota_{\mathcal{B}_\theta}$
Case 1	(B)	$\beta_\theta\,\overline{q}^2 - 2\gamma_\theta\,\overline{q} + 1$	$\overline{q}\iota_{\mathcal{B}_\theta}$
	(C)	$(1-\overline{q})^2$	$\overline{q}\iota_{\mathcal{B}_\theta}$
ILP	(A)	$\beta_\theta - 2\gamma_\theta + 1$	$\alpha\iota_{\mathcal{B}_\theta}/\overline{q}$
Case 2	(B)	$\beta_\theta - 2\gamma_\theta + 1$	$\iota_{\mathcal{B}_\theta}/\overline{q}$
	(C)	0	$\iota_{\mathcal{B}_\theta}/\overline{q}$
ILP	(A)	$\beta_\theta - 2\gamma_\theta + 1$	$[\alpha + 2(\gamma_\theta - \beta_\theta)]\iota_{\mathcal{B}_\theta}/\overline{q}$
Case 3	(B)	$\beta_\theta - 2\gamma_\theta + 1$	$[1 + 2(\gamma_\theta - \beta_\theta)]\iota_{\mathcal{B}_\theta}/\overline{q}$
	(C)	0	$\iota_{\mathcal{B}_\theta}/\overline{q}$
ILP	(A)	$\left(1-\gamma_\theta^2/\beta_\theta\right)$	$\alpha\gamma_\theta^2\iota_{\mathcal{B}_\theta}/(\overline{q}\beta_\theta^2)$
Case 4	(B)	$\left(1-\gamma_\theta^2/\beta_\theta\right)$	$\gamma_\theta^2\iota_{\mathcal{B}_\theta}/(\overline{q}\beta_\theta^2)$
	(C)	0	$\iota_{\mathcal{B}_\theta}/\overline{q}$
Opt. LSI	(A)	0	$\frac{\alpha}{\overline{q}}\int_{\breve{\mathcal{B}}}\frac{\lvert\breve{\Phi}(\breve{\sigma}_{\mathbf{e}_\mathrm{s}}\breve{\boldsymbol{\nu}})\rvert^{-2}\lvert\breve{Z}(\breve{\boldsymbol{\nu}})\rvert^2}{\lvert(\breve{\Lambda}*\breve{Q}*\breve{Z})(\breve{\boldsymbol{\nu}})\rvert^2}d\breve{\boldsymbol{\nu}}$
($\breve{\mathcal{B}}\subset\mathbb{R}^d$)	(B)	0	$\frac{1}{\overline{q}}\int_{\breve{\mathcal{B}}}\lvert\breve{\Phi}(\breve{\sigma}_{\mathbf{e}_\mathrm{s}}\breve{\boldsymbol{\nu}})\rvert^{-2}d\breve{\boldsymbol{\nu}}$
	(C)	0	$\iota_{\mathcal{B}}/\overline{q}$

reconstruction MSE is

$$\varepsilon_\mathrm{s} = c_0 + c_1\frac{1}{\iota_\lambda} + o\Big(\frac{1}{\iota_\lambda}\Big) \tag{62}$$

where the floor c_0 and the first order coefficient c_1 are specified in Table II for ILP interpolator and for optimal LSI interpolator with $\iota_{\mathcal{B}} \triangleq |\mathcal{B}|/(2B)^d$.[19]

Proof: For ILP interpolator, results follow from (53)–(57) by using normalized quantities. For optimal LSI interpolator, the normalized version of (60) results in

$$\varepsilon_\mathrm{s} = 1 - \int_{\breve{\mathcal{B}}}\frac{|\breve{Z}(\breve{\boldsymbol{\nu}})|^2}{1+\frac{\alpha}{\overline{q}\iota_\lambda}|\breve{\Phi}(\breve{\sigma}_{\mathbf{e}_\mathrm{s}}\breve{\boldsymbol{\nu}})|^{-2}|\left(\breve{\Lambda}*\breve{Q}*\breve{Z}\right)(\breve{\boldsymbol{\nu}})|^{-2}}d\breve{\boldsymbol{\nu}}$$

that, for $\iota_\lambda \to \infty$, leads to the expressions in row 5 of Table II. □

Remark 10: For homogeneous PSP without sample position errors, the ILP interpolator (typical choice for wireless sensor network applications) in cases 3 and 4 with $\iota_{\mathcal{B}_\theta} = \iota_{\mathcal{B}}$ is asymptotically optimum.

V. CASE STUDY

We now describe a case study for multidimensional random sampling under different conditions and, when present, with Gaussian distributed sample position errors. The considered sampled signal is that of the example in (2). Since the sampling intensity $\lambda(\mathbf{x})$ and the sample availability $q(\mathbf{x})$ are interchangeable in the presented Theorems,[20] without loss of generality consider the case $q(\mathbf{x}) = \overline{q}$.

Proposition 1 (ILP Interpolator): Under the hypothesis of Corollary 7 for zero-mean Gaussian IID sample position errors with normalized variance $\breve{\sigma}^2_{\mathbf{e}_\mathrm{s}}$, when the sampled signal has an ESD as in (3), the PSP intensity is $\lambda(\mathbf{x})$ as in (5), and the sample availability is $q(\mathbf{x}) = \overline{q}$, the reconstructed signal ESD results in

$$\breve{\mathcal{E}}_{\widehat{\mathbf{z}}}(\breve{\boldsymbol{\nu}}) = \frac{\overline{q}^2\,\iota_\lambda^2}{\breve{\kappa}_\theta^2}\,e^{-4\pi^2\breve{\sigma}^2_{\mathbf{e}_\mathrm{s}}\|\breve{\boldsymbol{\nu}}\|^2}\prod_{i=0}^{d-1}\frac{1}{2b_i}\left\{\mathrm{rect}\left(\frac{\breve{\nu}_i}{2b_i}\right) + \frac{a_i^2}{4}\left[\mathrm{rect}\left(\frac{\breve{\nu}_i}{2|b_i+b_{\lambda_i}|}\right) - \mathrm{rect}\left(\frac{\breve{\nu}_i}{2|b_i-b_{\lambda_i}|}\right)\right]\right\} + \frac{\overline{q}\,\iota_\lambda}{\breve{\kappa}_\theta^2}\,\mathbb{1}_{\breve{\mathcal{B}}_\theta}(\breve{\boldsymbol{\nu}})$$

and the signal reconstruction MSE is found to be (36) with

$$\alpha = 1 \tag{63a}$$

$$\beta_\theta = \prod_{i=0}^{d-1}\frac{1}{4\sqrt{\pi}b_i\breve{\sigma}_{\mathbf{e}_\mathrm{s}}}\left\{\mathrm{erf}\left(2\pi b_i\breve{\sigma}_{\mathbf{e}_\mathrm{s}}\right) + \frac{a_i^2}{4}\mathrm{erf}\left(2\pi|b_i+b_{\lambda_i}|\breve{\sigma}_{\mathbf{e}_\mathrm{s}}\right) - \frac{a_i^2}{4}\mathrm{erf}\left(2\pi|b_i-b_{\lambda_i}|\breve{\sigma}_{\mathbf{e}_\mathrm{s}}\right)\right\} \tag{63b}$$

$$\gamma_\theta = \prod_{i=0}^{d-1}\frac{1}{\sqrt{8\pi}\,b_i\breve{\sigma}_{\mathbf{e}_\mathrm{s}}}\,\mathrm{erf}\left(\sqrt{2}\,\pi b_i\breve{\sigma}_{\mathbf{e}_\mathrm{s}}\right). \tag{63c}$$

where $\mathrm{erf}(\cdot)$ is the Gaussian error function.

Example: Consider the setting of Proposition 1 with $\iota_{\mathcal{B}_\theta} = 25$ and κ_θ according to (55) since α, β_θ, and γ_θ are unknown to the interpolator.[21] The signal bandwidth-per-dimension is $B = 10^{-4}\,[\mathrm{m}^{-1}]$.

Fig. 4(a) shows the signal reconstruction MSE as a function of $\overline{\lambda}$ for $b_\lambda = 1/2$ and different values of $\breve{\sigma}_{\mathbf{e}_\mathrm{s}}$ and a. The case of homogeneous PSP without sample position errors ($a = 0, \breve{\sigma}_{\mathbf{e}_\mathrm{s}} = 0$) is also given as a benchmark. It can be observed that, while in the case of homogeneous PSP without sample position errors the signal reconstruction MSE is linearly decreasing with the average sampling intensity $\overline{\lambda}$ (consistently with [41]), both the inhomogeneity and the sample position errors generate an error floor. However, while the effect of the inhomogeneous amplitude parameter a is always appreciable, that of the normalized position error standard deviation $\breve{\sigma}_{\mathbf{e}_\mathrm{s}}$ is evident only with homogeneity ($a = 0$) or small inhomogeneity ($a = 0.01$). Note also that the effect on the signal reconstruction MSE of an inhomogeneity of 1% is almost equivalent to that of a position error of 5%.

Fig. 4(b) shows the signal reconstruction MSE as a function of $\breve{\sigma}_{\mathbf{e}_\mathrm{s}}$ for an average PSP intensity $\overline{\lambda} = 10^{-2}[\mathrm{m}^{-2}]$ and different values of a and b_λ. It can be observed that, in the homogeneous case ($a = 0$ or $b_\lambda = 0$) the effects of sample position errors become evident when $\breve{\sigma}_{\mathbf{e}_\mathrm{s}}$ is greater than 5% of the signal correlation distance (i.e., $1/2B$). Also, in the inhomogeneous case ($a > 0$ and $b_\lambda > 0$) the effects of sample position errors become relevant for lower $\breve{\sigma}_{\mathbf{e}_\mathrm{s}}$ and the behaviour of the signal reconstruction MSE shows a local minimum that is more evident for higher values of a. This can be attributed to the fact that, when samples are inhomogeneously distributed with low intensity, sample position uncertainties regularize the sample spatial

[19] For ILP interpolator cases 3 and 4, in which the signal band is known, $\iota_{\mathcal{B}_\theta} = \iota_{\mathcal{B}}$ can be considered. For optimal LSI interpolator, the signal $z(\mathbf{x})$, availability $q(\mathbf{x})$, and intensity $\lambda(\mathbf{x})$ are here considered strictly band-limited (i.e., $\breve{\mathcal{B}} \subset \mathbb{R}^d$).

[20] This is expected since the effect of $q(\mathbf{x})$ is to mark Π.

[21] The $\iota_{\mathcal{B}_\theta} = 25$ corresponds, e.g., to an oversampling factor of 5 for each dimension in $\mathbb{R}^2$, thus $\breve{\mathcal{B}}_\mathrm{s} \subseteq \breve{\mathcal{B}}_\theta$ for $b_\lambda \leq 2$.

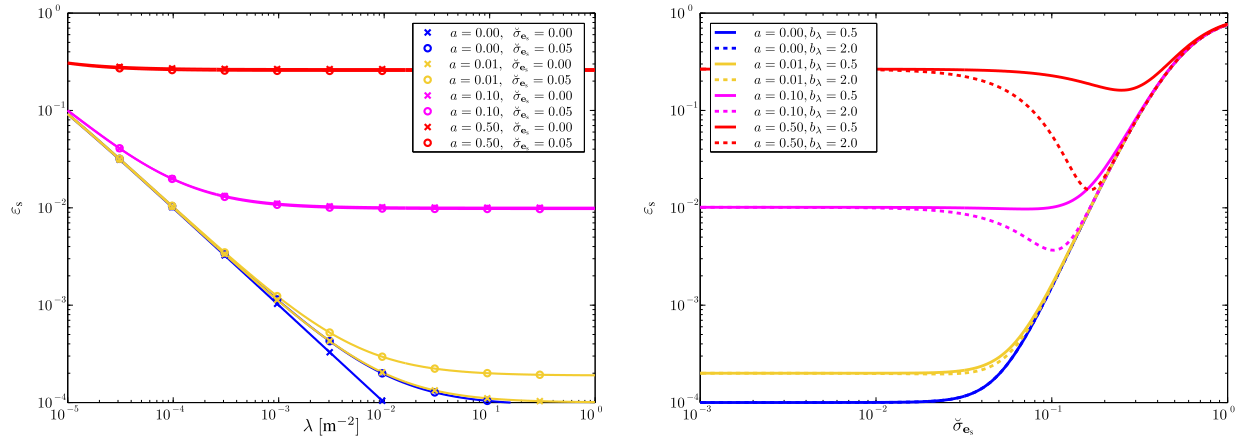

(a) Signal reconstruction MSE as a function of average PSP intensity $\bar{\lambda}$ for $b\lambda = 0.5$

(b) Signal reconstruction MSE as a function of normalized position error $\breve{\sigma}_{\mathbf{e}_s}$ with $\bar{\lambda} = 10^{-2}$ m^{-2}

Fig. 4. Signal reconstruction MSE as a function of average PSP intensity $\bar{\lambda}$ and normalized position error $\breve{\sigma}_{\mathbf{e}_s}$ with the following parameters: $d = 2$, $B = 10^{-4}$ [m^{-1}], $\iota_{\mathcal{B}_\theta} = 25$, $p_n = p = 10^{-3}, \forall n$.

distribution. For high $\breve{\sigma}_{\mathbf{e}_s}$, however, all the curves approach to an asymptotic value.

Proposition 2 (Optimal LSI Interpolator): In the setting of Proposition 1, the optimal LSI interpolator leads to

$$\varepsilon_s = 1 - \int_{-b_0}^{b_0} \int_{-b_1}^{b_1} \cdots \int_{-b_{d-1}}^{b_{d-1}} \frac{d\hat{\nu}_0 d\hat{\nu}_1 \ldots d\hat{\nu}_{d-1}}{\zeta(\hat{\nu}_0, \hat{\nu}_1, \ldots, \hat{\nu}_{d-1})} \tag{64}$$

where

$$\zeta\left(\hat{\nu}_0, \hat{\nu}_1, \ldots, \hat{\nu}_{d-1}\right) \triangleq \frac{1}{\bar{q}\iota_\lambda} \prod_{i=0}^{d-1} \frac{2b_i\, e^{4\pi^2 \breve{\sigma}_{\mathbf{e}_s}^2 \breve{\nu}_i^2}}{1 + \frac{a_i^2}{4} \psi_{\frac{b_{\lambda_i}}{2b_i}}\left(\frac{\breve{\nu}_i}{2b_i}\right)} + \prod_{i=0}^{d-1} 2b_i$$

and $\psi_b(x) \triangleq [\mathrm{rect}(x-b) - \mathrm{rect}(x+b)]^2$.

Remark 11: For homogeneous PSP ($a_i = 0$ or $b_{\lambda_i} = 0$) in the absence of sample position errors ($\breve{\sigma}_{\mathbf{e}_s} = 0$), (64) becomes

$$\varepsilon_s = \frac{\prod_{i=0}^{d-1}(2b_i)}{\bar{q}\iota_\lambda + \prod_{i=0}^{d-1}(2b_i)} \tag{65}$$

that, for one dimension ($d = 1$ thus $b_0 = 1/2$) is consistent with the result in [77] for a sinc-type signal reconstructed by an optimal linear time-invariant (LTI) interpolator in the case of stationary PSP.

Proposition 3 (Optimal LSI Interpolator—Homogeneous PSP—Asymptotic Analysis): In the setting of Proposition 2 with homogeneous PSP, the signal reconstruction MSE results in

$$\varepsilon_s = \frac{1}{\bar{q}\iota_\lambda} \prod_{i=0}^{d-1} \frac{1}{2\sqrt{\pi}\,\breve{\sigma}_{\mathbf{e}_s}} \mathrm{erfi}\left(2\pi b_i \breve{\sigma}_{\mathbf{e}_s}\right) + o\left(\frac{1}{\iota_\lambda}\right) \tag{66}$$

where $\mathrm{erfi}(z) \triangleq -\jmath\,\mathrm{erf}(\jmath z)$.

Example: Consider the signal as in (2) sampled by an homogeneous PSP. Fig. 5(a) and (b) show the signal reconstruction MSE as a function of the normalized PSP intensity ι_λ for the homogeneous case in $\mathbb{R}^2$ with the different interpolators discussed in Section IV. When the signal band is unknown, an oversampling factor $\iota_{\mathcal{B}_\theta} = 25$ is considered. In the absence of sample position errors, Fig. 5(a), the only knowledge of the average sample density (Case 1) shows an error floor. If also the band of the signal to be reconstructed is known to the interpolator (Case 3), the signal reconstruction MSE is reduced due to the lower amount of sampling noise[22] collected by an ILP interpolator with oversampling factor $\iota_{\mathcal{B}_\theta} = 1$. Case 4 coincides with Case 3 in the absence of sample position errors, as expected. The signal reconstruction MSE with optimal LSI interpolator case coincides in this example to that with optimized ILP interpolator, as it can be noticed by comparing (56) for $\alpha = \beta_\theta = \gamma_\theta = 1$(homogeneous case without position errors) and $\iota_{\mathcal{B}_\theta} = \iota_{\mathcal{B}} = 1$(knowledge of signal band) to (65) for $b_0 = b_1 = 1/2$. In the presence of sample position errors, an error floor is introduced for all the ILP cases. Note that the advantage of the knowledge of sample loss (Case 2) becomes irrelevant, while that of the signal band (Case 3) is relevant only for relatively small sample density. The optimized ILP interpolator with the knowledge of the position error statistic performs closely to the optimal LSI interpolator for $\iota_\lambda < 10^6$, while for higher values an error floor arises (even if lower than the other ILP cases).

Proposition 4 (Optimal LSI Interpolator—Inhomogeneous PSP—Asymptotic Analysis): In the setting of Proposition 2, the signal reconstruction MSE results in

$$\varepsilon_s = \frac{1}{\bar{q}\,\iota_\lambda} \prod_{i=0}^{d-1} \int_{-b_i}^{b_i} \frac{e^{4\pi^2 \breve{\sigma}_{\mathbf{e}_s}^2 \breve{\nu}_i^2} d\breve{\nu}_i}{1 + \frac{a_i^2}{4}\,\psi_{\frac{b_{\lambda_i}}{2b_i}}\left(\frac{\breve{\nu}_i}{2b_i}\right)} + o\Big(\frac{1}{\iota_\lambda}\Big). \tag{67}$$

Example: Consider the signal as in (2) sampled by an inhomogeneous PSP with intensity given by (5). The oversampling factor is $\iota_{\mathcal{B}_\theta} = 25$ for ILP interpolator cases 1 and 2, while for ILP cases 3 and 4, the interpolator band is assumed to be the minimal such that $\breve{\mathcal{B}}_s \subseteq \breve{\mathcal{B}}_\theta$ (i.e., $\iota_{\mathcal{B}_\theta} = 1.21$ for $b_\lambda = 0.05$). Fig. 5(c) and (d) show the impact of inhomogeneity on ε_s. Both in the absence and in the presence of sample position errors, it can be observed that the error floors for the ILP interpolators are higher than in the homogeneous case and that performance close to the case of optimal LSI can be reached for low ι_λ. In

[22]We recall that the homogeneous PSP introduces a sampling noise in the sampled signal spectrum, as shown in Fig. 1(b).

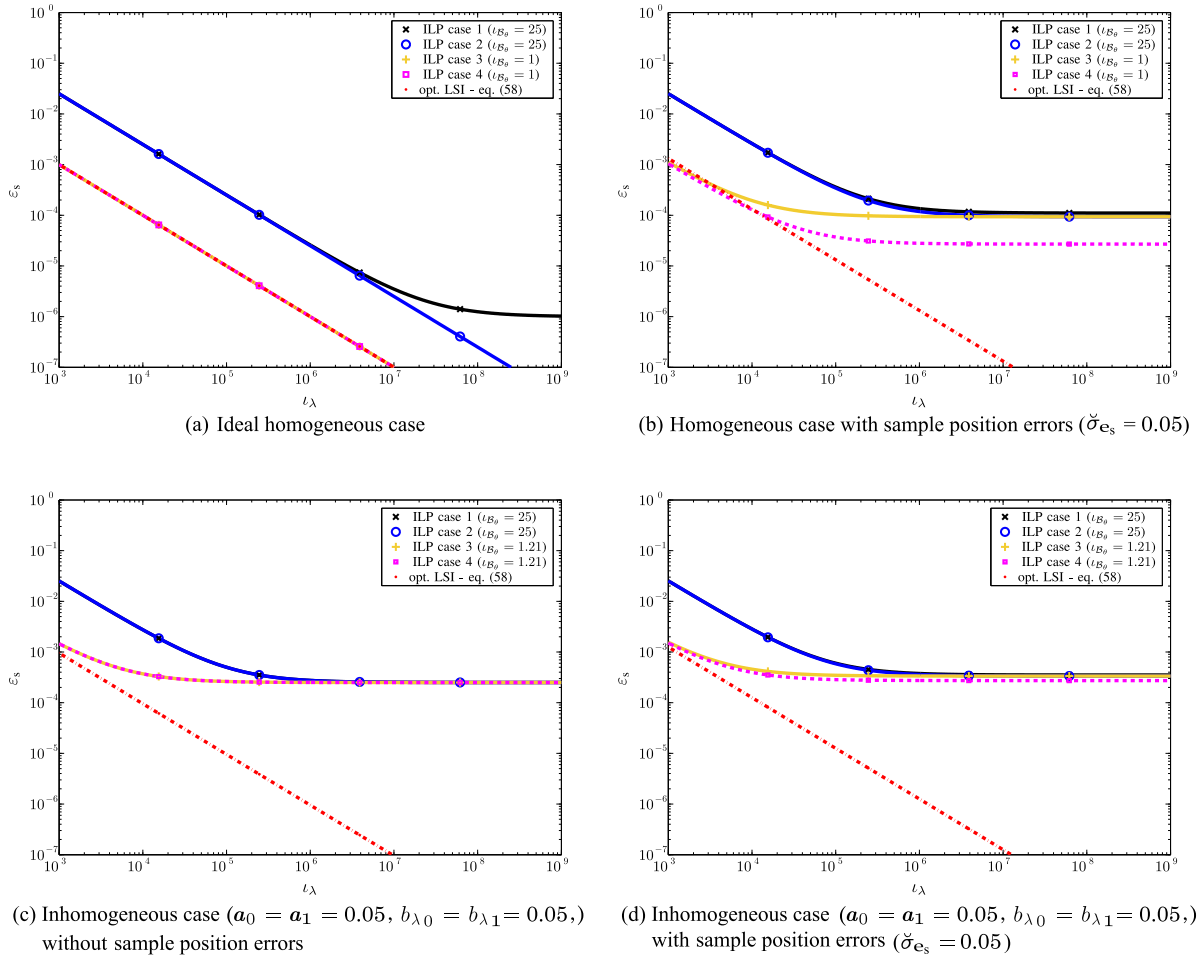

(a) Ideal homogeneous case

(b) Homogeneous case with sample position errors ($\breve{\sigma}_{\mathbf{e}_s} = 0.05$)

(c) Inhomogeneous case ($\boldsymbol{a}_0 = \boldsymbol{a}_1 = 0.05$, $b_{\lambda 0} = b_{\lambda 1} = 0.05$,) without sample position errors

(d) Inhomogeneous case ($\boldsymbol{a}_0 = \boldsymbol{a}_1 = 0.05$, $b_{\lambda 0} = b_{\lambda 1} = 0.05$,) with sample position errors ($\breve{\sigma}_{\mathbf{e}_s} = 0.05$)

Fig. 5. Signal reconstruction MSE in $\mathbb{R}^2$ (corresponding to the case of Fig. 1) for $p_n = p = 10^{-3}, \forall n$.

such case, the knowledge of the signal band and that of the inhomogeneous PSP intensity function (case 3) are significant. In the presence of sample position errors, their statistical knowledge (case 4) provides a negligible advantage.

VI. Final Remark

This paper provides a general analysis for sampling and reconstruction of a finite-energy signal in $\mathbb{R}^d$ based on a finite set of samples randomly gathered in a presence of sample position uncertainties. The reconstructed signal ESD and reconstruction MSE are derived accounting for: (i) signal properties such as signal spectrum and spatial correlation; (ii) sampling properties such as inhomogeneous sample spatial distribution, sample availability, and non-ideal knowledge of sample positions; and (iii) interpolation filtering. The main results are listed below.

1) The reconstructed signal ESD derived in Theorem 1 shows how the ESD is enlarged by inhomogeneous PSP and distorted in-band by imperfect knowledge of samples positions. The former effect requires an interpolator with bandwidth per dimension greater than Nyquist frequency, whereas the latter can be mitigated through equalization.
2) A general expression for the signal reconstruction MSE is derived in Theorem 3 extending the one for the case of homogeneous PSP with perfect knowledge of the samples positions to the case of inhomogeneous PSP with imperfect knowledge of samples positions. Such expression generalizes a known result by mean of three parameters $(\alpha, \beta_\theta, \gamma_\theta)$ that are obtained as a function of signal and sampling properties. In addition, the parameters are determined for cases of practical interest.
3) The reconstruction MSE parameters are obtained in Theorem 4. Parameter α depends on the sampling intensity function, the sample availability function, and the signal to be reconstructed. Parameters β_θ and γ_θ depend on the Φ-mean of modified versions of the signal ESD (Φ is related to the characteristic function of sample position errors), the normalized standard deviation of sample position errors $\breve{\sigma}_{\mathbf{e}_s}$, and the spectra of sampling intensity and sample availability.
4) It was know that one-dimensional homogeneous PSP introduces a white sampling noise, and that the condition for the signal-to-sampling noise ratio (evaluated in the signal bandwidth) greater than 1 is average intensity of available sampling greater than or equal to the Nyquist rate, i.e., $\overline{q}\overline{\lambda} \geq 2B$. We have demonstrated that for d-dimensional inhomogeneous PSP with sample position errors and generic LSI interpolator, the condition for the signal-to-sampling noise ratio at the interpolator's output greater than 1 is $\overline{q}\overline{\lambda} \geq \alpha\,|\mathcal{B}_\theta|/\beta_\theta$, where $|\mathcal{B}_\theta|$ is

the Lebesgue measure of the interpolator d-dimensional band.

5) The optimal LSI interpolator minimizing the signal reconstruction MSE is derived in Theorem 5 and the corresponding signal reconstruction MSE is given in Theorem 6. Such interpolator can compensate both sample inhomogeneity and position errors. In the inhomogeneous case, the optimal LSI is not practically realizable as it would require the prior knowledge of the signal to be reconstructed. Moreover, it is shown that the widely adopted ILP interpolator can be considered asymptotically optimal in the case of homogeneous sampling without sample position errors only, as in non-ideal condition (inhomogeneous PSP and/or sample position errors) it generates a reconstruction MSE error floor.
6) It is demonstrated to which extent sample position errors affect the signal reconstruction MSE based on the ratio between the error standard deviation and the spatial correlation of the signal per dimension. When the sample position errors are Gaussian distributed, β_θ and γ_θ reduce to the Weierstrass transform (with parameter inversely proportional to the square of $\breve{\sigma}_{\mathbf{e}_s}$) of a modified version of the signal ESD. Moreover, when the spatial sample distribution and the sample availability are homogeneous and no sample position errors are present, the expression of the signal reconstruction MSE and that of optimal LSI interpolator reduce to known results as subcases.

Appendix A
Proof of Lemma 1

Proof: In the sense of distributions, from the properties of Dirac delta generalized function, $\mathsf{y}_{\mathcal{L}}(\mathbf{x}) = y(\mathbf{x}) \sum_{n\in\mathcal{N}_{\mathbf{\Pi}}} \mathsf{a}_n \delta(\mathbf{x}-\mathsf{x}_n) = \sum_{n\in\mathcal{N}_{\mathbf{\Pi}}} \mathsf{a}_n y(\mathsf{x}_n)\delta(\mathbf{x}-\mathsf{x}_n)$. By applying the FT, $\mathsf{Y}_{\mathcal{L}}(\boldsymbol{\nu}) \triangleq \boldsymbol{\mathcal{F}}\{\mathsf{y}_{\mathcal{L}}(\mathbf{x})\}(\boldsymbol{\nu}) = \sum_{n\in\mathcal{N}_{\mathbf{\Pi}}} \mathsf{a}_n y(\mathsf{x}_n) e^{-\jmath 2\pi \boldsymbol{\nu}\cdot\mathsf{x}_n}$, thus

$$\mathcal{E}_{\mathsf{y}_{\mathcal{L}}}(\boldsymbol{\nu}) = \mathbb{E}\left\{|\mathsf{Y}_{\mathcal{L}}(\boldsymbol{\nu})|^2\right\} = \mathbb{E}\Big\{\Big|\sum_{n\in\mathcal{N}_{\mathbf{\Pi}}} a_n\, y(\mathsf{x}_n)\, e^{-\jmath 2\pi\boldsymbol{\nu}\cdot\mathsf{x}_n}\Big|^2\Big\}$$

that results in (14). By substituting (6) and $\mu_{\mathcal{L}}(\mathbf{x}) = \mathbb{E}\{\mathcal{L}(\mathbf{x})\}$ in (13), and exploiting the linearity of integral operator, it is

$$\Upsilon_{\mathcal{L}}[y] = \mathbb{E}\Big\{\int_{\mathbb{R}^d} |y(\mathbf{x})|^2 \sum_{n\in\mathcal{N}_{\mathbf{\Pi}}} \mathsf{a}_n \delta(\mathbf{x}-\mathsf{x}_n)\, d\mathbf{x}\Big\}$$

which, from the properties of Dirac delta generalized function and the independence of a_n's from $\mathbf{\Pi}$, results in (15). □

Appendix B
Proof of Lemma 2

Proof: By generalizing the result of [80] for an inhomogeneous PSP $\mathcal{S}$ in $\mathbb{R}^d$ with intensity $\lambda(\mathbf{x})$, it is

$$\mu_{\mathcal{S}}(\mathbf{x}) = \lambda(\mathbf{x}) \tag{68a}$$

$$R_{\mathcal{S}}(\mathbf{x},\boldsymbol{\tau}) = \lambda(\mathbf{x})\,\lambda(\mathbf{x}-\boldsymbol{\tau}) + \lambda(\mathbf{x}-\boldsymbol{\tau})\,\delta(\boldsymbol{\tau})\,. \tag{68b}$$

The (18a) is obtained by Fourier transforming (68a). Since $\mathcal{S}$ is non-stationary, the ESD of $\mathsf{y}_{\mathcal{S}}(\mathbf{x})$ cannot be directly evaluated as a convolution between the ESD of $y(\mathbf{x})$ and the PSD of $\mathcal{S}$, but has to be computed by Fourier-transforming $C_{\mathsf{y}_{\mathcal{S}}}(\boldsymbol{\tau}) \triangleq \int_{\mathbb{R}^d} R_{\mathsf{y}_{\mathcal{S}}}(\mathbf{x},\boldsymbol{\tau})\, d\mathbf{x}$ where

$$R_{\mathsf{y}_{\mathcal{S}}}(\mathbf{x},\boldsymbol{\tau}) = y(\mathbf{x})\, y^\dagger(\mathbf{x}-\boldsymbol{\tau})\, R_{\mathcal{S}}(\mathbf{x},\boldsymbol{\tau})\,. \tag{69}$$

By substituting (68b) in (69) we obtain

$$\begin{aligned} C_{\mathsf{y}_{\mathcal{S}}}(\boldsymbol{\tau}) &= \int_{\mathbb{R}^d} \lambda(\mathbf{x})\, y(\mathbf{x})\, \lambda(\mathbf{x}-\boldsymbol{\tau})\, y^\dagger(\mathbf{x}-\boldsymbol{\tau})\, d\mathbf{x} \\ &\quad + \delta(\boldsymbol{\tau}) \int_{\mathbb{R}^d} y(\mathbf{x})\, y^\dagger(\mathbf{x}-\boldsymbol{\tau})\, \lambda(\mathbf{x}-\boldsymbol{\tau})\, d\mathbf{x} \\ &= \left(y_\lambda * y^\dagger_{\lambda-}\right)(\boldsymbol{\tau}) + \delta(\boldsymbol{\tau})\, \left(y * y^\dagger_{\lambda-}\right)(\boldsymbol{\tau}) \end{aligned} \tag{70}$$

where $y_\lambda(\mathbf{x}) \triangleq \lambda(\mathbf{x})\, y(\mathbf{x})$ and $y_{\lambda-}(\mathbf{x}) \triangleq y_\lambda(-\mathbf{x})$. By Fourier transforming (70) and using the fact that $\boldsymbol{\mathcal{F}}\{\delta(\boldsymbol{\tau})\,(y * y^\dagger_{\lambda-})(\boldsymbol{\tau})\}(\mathbf{0}) = (y * y^\dagger_{\lambda-})(\mathbf{0}) = \int_{\mathbb{R}^d} \lambda(\mathbf{x})|y(\mathbf{x})|^2 d\mathbf{x}$, we obtain

$$\mathcal{E}_{\mathsf{z}_{\mathcal{S}}}(\boldsymbol{\nu}) = |(\Lambda * Y)(\boldsymbol{\nu})|^2 + \int_{\mathbb{R}^d} \lambda(\mathbf{x})\, |y(\mathbf{x})|^2 d\mathbf{x}\,.$$

This results in (18b) using (68a) and (17). From (15) with $\mathsf{a}_n = 1\,\forall n \in \mathcal{N}_{\mathbf{\Pi}}$ ($\mathcal{L} \equiv \mathcal{S}$ and $q_n = 1\,\forall n$) we obtain (19). □

Appendix C
Proof of Lemma 3

Proof: From (14) with $y(\mathbf{x}) = z(\mathbf{x})$, the independence of a_n's from $\mathbf{\Pi}$, and $\mathbb{E}\{\mathsf{a}_n^2\} = q_n$, we have

$$\begin{aligned} \mathcal{E}_{\mathsf{z}_{\mathcal{L}}}(\boldsymbol{\nu}) &= \mathbb{E}\Big\{\sum_{n\in\mathcal{N}_{\mathbf{\Pi}}} \sum_{\substack{k\in\mathcal{N}_{\mathbf{\Pi}} \\ k\neq n}} q_n\, q_k\, z(\mathsf{x}_n)\, z^\dagger(\mathsf{x}_k)\, e^{-\jmath 2\pi\boldsymbol{\nu}\cdot(\mathsf{x}_n-\mathsf{x}_k)}\Big\} \\ &\quad + \mathbb{E}\Big\{\sum_{n\in\mathcal{N}_{\mathbf{\Pi}}} q_n\, |z(\mathsf{x}_n)|^2\Big\} \\ &= \mathbb{E}\Big\{\sum_{n\in\mathcal{N}_{\mathbf{\Pi}}} \sum_{k\in\mathcal{N}_{\mathbf{\Pi}}} z_{\mathrm{q}}(\mathsf{x}_n)\, z^\dagger_{\mathrm{q}}(\mathsf{x}_k)\, e^{-\jmath 2\pi\boldsymbol{\nu}\cdot(\mathsf{x}_n-\mathsf{x}_k)}\Big\} \\ &\quad - \mathbb{E}\Big\{\sum_{n\in\mathcal{N}_{\mathbf{\Pi}}} |z_{\mathrm{q}}(\mathsf{x}_n)|^2\Big\} + \mathbb{E}\Big\{\sum_{n\in\mathcal{N}_{\mathbf{\Pi}}} q_n\, |z(\mathsf{x}_n)|^2\Big\}\,. \end{aligned}$$

This results in (20) by using Lemma 1 with $y(\mathbf{x}) = z_{\mathrm{q}}(\mathbf{x})$ and $\mathcal{L} \equiv \mathcal{S}$ ($\mathsf{a}_n = 1\,\forall n \in \mathcal{N}_{\mathbf{\Pi}}$) for the first two terms, and by using (15) with $y(\mathbf{x}) = z(\mathbf{x})$ for the third term. □

Appendix D
Proof of Lemma 4

Proof: Note that, by using the definition of FT and the properties of Dirac delta generalized function, it is

$$\begin{aligned} &\boldsymbol{\mathcal{F}}\Big\{z(\mathbf{x}) \sum_{n\in\mathcal{N}_{\mathbf{\Pi}}} \mathsf{a}_n \delta(\mathbf{x}-\mathsf{x}_n)\Big\}(\boldsymbol{\nu}) \\ &\qquad = \sum_{n\in\mathcal{N}_{\mathbf{\Pi}}} \mathsf{a}_n\, z(\mathsf{x}_n)\, e^{-\jmath 2\pi\boldsymbol{\nu}\cdot\mathsf{x}_n}\,. \end{aligned} \tag{71}$$

This, together with (8b) and the independence of $\mathbf{e}_{\mathrm{s}n}$'s, a_n's, and $\mathbf{\Pi}$, gives

$$\begin{aligned} \mathcal{U}_{\mathsf{z}_{\mathrm{u}}}(\boldsymbol{\nu}) &= \Phi_{\mathbf{e}_{\mathrm{s}}}(\boldsymbol{\nu})\, \mathbb{E}\Big\{\sum_{n\in\mathcal{N}_{\mathbf{\Pi}}} \mathsf{a}_n\, z(\mathsf{x}_n)\, e^{-\jmath 2\pi\boldsymbol{\nu}\cdot\mathsf{x}_n}\Big\} \\ &= \Phi_{\mathbf{e}_{\mathrm{s}}}(\boldsymbol{\nu})\, \boldsymbol{\mathcal{F}}\{z(\mathbf{x})\, \mu_{\mathcal{L}}(\mathbf{x})\}(\boldsymbol{\nu}) \end{aligned} \tag{72}$$

that, through the convolution properties, gives (21a). From the aforementioned independence property and Lemma 1, it is

$$\mathcal{E}_{\mathsf{z}_\mathrm{u}}(\boldsymbol{\nu}) = \mathbb{E}\Big\{ \sum_{n\in\mathcal{N}_\mathbf{\Pi}} \mathsf{a}_n^2 \,|z(\mathsf{x}_n)|^2 \Big\} + \mathbb{E}\Big\{ \sum_{n\in\mathcal{N}_\mathbf{\Pi}} \sum_{\substack{k\in\mathcal{N}_\mathbf{\Pi}\\ k\neq n}} \mathsf{a}_n \mathsf{a}_k \times z(\mathsf{x}_n)\, z^\dagger(\mathsf{x}_k)\, e^{-\jmath 2\pi \boldsymbol{\nu}\cdot(\mathsf{x}_n-\mathsf{x}_k)}\, \Phi_{\mathbf{e}_\mathrm{s}}(\boldsymbol{\nu})\, \Phi^\dagger_{\mathbf{e}_\mathrm{s}}(\boldsymbol{\nu}) \Big\}$$

$$= \mathbb{E}\Big\{ \sum_{n\in\mathcal{N}_\mathbf{\Pi}} q_n |z(\mathsf{x}_n)|^2 \Big\} - |\Phi_{\mathbf{e}_\mathrm{s}}(\boldsymbol{\nu})|^2 \Big\{ \sum_{n\in\mathcal{N}_\mathbf{\Pi}} q_n |z(\mathsf{x}_n)|^2 \Big\} + |\Phi_{\mathbf{e}_\mathrm{s}}(\boldsymbol{\nu})|^2 \mathbb{E}\Big\{ \sum_{n\in\mathcal{N}_\mathbf{\Pi}} \sum_{k\in\mathcal{N}_\mathbf{\Pi}} \mathsf{a}_n \mathsf{a}_k z(\mathsf{x}_n)\, z^\dagger(\mathsf{x}_k)\, e^{-\jmath 2\pi \boldsymbol{\nu}\cdot(\mathsf{x}_n-\mathsf{x}_k)} \Big\}$$

that results in (21b) by (14) and (15) with $y(\mathbf{x}) = z(\mathbf{x})$. □

Appendix E
Proof of Theorem 1

Proof: From (20) and (21b) we have

$$\mathcal{E}_{\mathsf{z}_\mathrm{u}}(\boldsymbol{\nu}) = |\Phi_{\mathbf{e}_\mathrm{s}}(\boldsymbol{\nu})|^2 \mathcal{E}_{z_\mathrm{qs}}(\boldsymbol{\nu}) - |\Phi_{\mathbf{e}_\mathrm{s}}(\boldsymbol{\nu})|^2 \Upsilon_{\mathcal{S}}[z_\mathrm{q}] + \Upsilon_{\mathcal{L}}[z]\,.$$

From (18b) with $y(\mathbf{x}) = z_\mathrm{q}(\mathbf{x})$ it follows

$$\mathcal{E}_{\mathsf{z}_\mathrm{u}}(\boldsymbol{\nu}) = |\Phi_{\mathbf{e}_\mathrm{s}}(\boldsymbol{\nu})|^2 |(\Lambda * Q * Z)(\boldsymbol{\nu})|^2 + \Upsilon_{\mathcal{L}}[z]\,. \tag{73}$$

From (15) with $y(\mathbf{x}) = z(\mathbf{x})$ and from (19) with $y(\mathbf{x}) = \sqrt{q(\mathbf{x})} z(\mathbf{x})$, we obtain

$$\Upsilon_{\mathcal{L}}[z] = \Upsilon_{\mathcal{S}}[\sqrt{q} z] = \mathbb{E}\Big\{ \sum_{n\in\mathcal{N}_\mathbf{\Pi}} q_n |z(\mathsf{x}_n)|^2 \Big\}. \tag{74}$$

By using (17) with $y(\mathbf{x}) = \sqrt{q(\mathbf{x})} z(\mathbf{x})$ and inverse FT of (18a), (74) leads to

$$\Upsilon_{\mathcal{L}}[z] = \int_{\mathbb{R}^d} \lambda(\mathbf{x})\, q(\mathbf{x})\, |z(\mathbf{x})|^2 d\mathbf{x}. \tag{75}$$

Then, (22) is obtained from (9), (23), (73), and (75). □

Appendix F
Proof of Theorem 2

Proof: Using the properties of the convolution operator for two generic functions $F(\boldsymbol{\nu})$ and $G(\boldsymbol{\nu})$, it can be seen that

$$\frac{\left[F(\boldsymbol{u}) * G\left(\frac{\boldsymbol{u}}{2B}\right)\right](\boldsymbol{\nu})}{(2B)^d} = \left[F(2B\boldsymbol{u}) * G(\boldsymbol{u})\right]\left(\frac{\boldsymbol{\nu}}{2B}\right). \tag{76}$$

From (25a), (25b), (76) with $F(\cdot) = \Lambda(\cdot)$ and $G(\cdot) = \breve{Q}(\cdot)$, and (76) with $F(\cdot) = Z(\cdot)$ and $G(\cdot) = (\breve{\Lambda} * \breve{Q})(\cdot)$, it is

$$(\Lambda * Q * Z)(\boldsymbol{\nu}) = \overline{q}\,\overline{\lambda} \frac{\sqrt{E_z}}{(2B)^{\frac{d}{2}}} \left(\breve{\Lambda} * \breve{Q} * \breve{Z}\right)\left(\frac{\boldsymbol{\nu}}{2B}\right). \tag{77}$$

From (11a), (28), (26b), (27a), (27b), and (77), the (22) results in (29). □

Appendix G
Proof of Theorem 3

Proof: By using (9), (21a) and (21b) in (31), and by applying the Parseval relation, we obtain

$$\begin{aligned}\varepsilon_\mathrm{s} &= \frac{\int_{\mathbb{R}^d} |z(\mathbf{x})|^2 d\mathbf{x}}{E_z} + \frac{\int_{\mathbb{R}^d} \mathbb{E}\left\{ |(\mathsf{z}_\mathrm{u} * \theta)(\mathbf{x})|^2 \right\} d\mathbf{x}}{E_z} - \frac{2\Re\left\{ \int_{\mathbb{R}^d} \mathbb{E}\left\{ (\mathsf{z}_\mathrm{u} * \theta)(\mathbf{x}) \right\} z^\dagger(\mathbf{x})\, d\mathbf{x} \right\}}{E_z} \\ &= 1 + \frac{1}{E_z} \int_{\mathbb{R}^d} |\Theta(\boldsymbol{\nu})|^2 \mathcal{E}_{\mathsf{z}_\mathrm{u}}(\boldsymbol{\nu})\, d\boldsymbol{\nu} - \frac{2}{E_z} \int_{\mathbb{R}^d} \Re\left\{ \Theta(\boldsymbol{\nu})\, \mathcal{U}_{\mathsf{z}_\mathrm{u}}(\boldsymbol{\nu})\, Z^\dagger(\boldsymbol{\nu}) \right\} d\boldsymbol{\nu}\,. \end{aligned} \tag{78}$$

By applying (7), (18a), (21a), and (73) to (78), the signal reconstruction MSE can be written as

$$\begin{aligned}\varepsilon_\mathrm{s} = 1 &+ \frac{\Upsilon_{\mathcal{L}}[z]}{E_z} \int_{\mathbb{R}^d} |\Theta(\boldsymbol{\nu})|^2 d\boldsymbol{\nu} \\ &+ \frac{1}{E_z} \int_{\mathbb{R}^d} |\Theta(\boldsymbol{\nu})|^2 |\Phi_{\mathbf{e}_\mathrm{s}}(\boldsymbol{\nu})|^2 |(\Lambda * Q * Z)(\boldsymbol{\nu})|^2 d\boldsymbol{\nu} \\ &- \frac{2}{E_z} \int_{\mathbb{R}^d} \Re\left\{ \Theta(\boldsymbol{\nu})\, \Phi_{\mathbf{e}_\mathrm{s}}(\boldsymbol{\nu})\, (\Lambda * Q * Z)(\boldsymbol{\nu})\, Z^\dagger(\boldsymbol{\nu}) \right\} d\boldsymbol{\nu}\,. \end{aligned}$$

that results in (32) from (10) and (75). □

Appendix H
Proof of Theorem 4

Proof: First apply the Parseval relation to (23), then (37a) is obtained from (35) after using (76) with $F(\cdot) = \Lambda(\cdot)$, $G(\cdot) = \breve{Q}(\cdot)$ and with $F(\cdot) = Z^\dagger(\cdot), G(\cdot) = \breve{Z}_-(\cdot)$. Equations (37b) and (37c) are obtained from (35) after substituting (26b), (27a), and (77) in (33a) and (33b), respectively. From (11a), (11b), and (27b), the (32) results in (36). □

Appendix I
Proof of Theorem 5

Proof: Consider the isometry between every generic finite-energy random process $f(\mathbf{x})$ and the corresponding vector $\underline{f}$. By establishing a metric defined by the scalar product as $\langle \underline{f}, \underline{g} \rangle \triangleq \mathbb{E}\left\{ \int_{\mathbb{R}^d} f(\mathbf{x})\, g^\dagger(\mathbf{x})\, d\mathbf{x} \right\}$, it can be shown that the LSI minimizing the signal reconstruction MSE results in

$$\Theta(\boldsymbol{\nu}) = \frac{Z(\boldsymbol{\nu})\, \mathcal{U}^\dagger_{\mathsf{z}_\mathrm{u}}(\boldsymbol{\nu})}{\mathcal{E}_{\mathsf{z}_\mathrm{u}}(\boldsymbol{\nu})}. \tag{79}$$

By (7), (18a), and (21a) it is

$$\mathcal{U}_{\mathsf{z}_\mathrm{u}}(\boldsymbol{\nu}) = \Phi_{\mathbf{e}_\mathrm{s}}(\boldsymbol{\nu})\, (\Lambda * Q * Z)(\boldsymbol{\nu})\,. \tag{80}$$

By substituting (73), (75), (23), and (80) in (79), we obtain (58). It follows that

$$\kappa_\theta = \frac{\left| \int_{\mathbb{R}^d} q(\mathbf{x})\, \lambda(\mathbf{x})\, z(\mathbf{x})\, d\mathbf{x} \right|^2 + \int_{\mathbb{R}^d} q(\mathbf{x})\, \lambda(\mathbf{x})\, |z(\mathbf{x})|^2 d\mathbf{x}}{\int_{\mathbb{R}^d} q(\mathbf{x})\, \lambda(\mathbf{x})\, z^\dagger(\mathbf{x})\, d\mathbf{x} \int_{\mathbb{R}^d} z(\mathbf{x})\, d\mathbf{x}} \tag{81}$$

and

$$|\mathcal{B}_\theta| = \kappa_\theta^2 \int_{\mathbb{R}^d} \frac{|\Phi_{\mathbf{e}_s}(\boldsymbol{\nu})|^2 |(\Lambda * Q * Z)(\boldsymbol{\nu})|^2 |Z(\boldsymbol{\nu})|^2}{\left[|\Phi_{\mathbf{e}_s}(\boldsymbol{\nu})|^2 |(\Lambda * Q * Z)(\boldsymbol{\nu})|^2 + \alpha \overline{q}\overline{\lambda} E_z\right]^2} d\boldsymbol{\nu}. \tag{82}$$

□

Appendix J
Proof of Theorem 6

Proof: By substituting (58) in (33a) and (33b), it is

$$\frac{\beta_\theta}{\kappa_\theta^2} = \frac{1}{\overline{q}^2 \overline{\lambda}^2 E_z} \int_{\mathbb{R}^d} \frac{|\Phi_{\mathbf{e}_s}(\boldsymbol{\nu})|^4 |(\Lambda * Q * Z)(\boldsymbol{\nu})|^4 |Z(\boldsymbol{\nu})|^2 d\boldsymbol{\nu}}{\left[|\Phi_{\mathbf{e}_s}(\boldsymbol{\nu})|^2 |(\Lambda * Q * Z)(\boldsymbol{\nu})|^2 + \alpha \overline{q}\overline{\lambda} E_z\right]^2} \tag{83a}$$

$$\frac{\gamma_\theta}{\kappa_\theta} = \frac{1}{\overline{q}\overline{\lambda} E_z} \int_{\mathbb{R}^d} \frac{|\Phi_{\mathbf{e}_s}(\boldsymbol{\nu})|^2 |(\Lambda * Q * Z)(\boldsymbol{\nu})|^2 |Z(\boldsymbol{\nu})|^2}{|\Phi_{\mathbf{e}_s}(\boldsymbol{\nu})|^2 |(\Lambda * Q * Z)(\boldsymbol{\nu})|^2 + \alpha \overline{q}\overline{\lambda} E_z} d\boldsymbol{\nu}. \tag{83b}$$

From (82) and (83a), it is $\alpha \frac{|\mathcal{B}_\theta|}{\kappa_\theta^2} + \overline{q}\overline{\lambda} \frac{\beta_\theta}{\kappa_\theta^2} = \frac{\gamma_\theta}{\kappa_\theta}$ that substituted in (32) gives $\varepsilon_s = 1 - \overline{q}\overline{\lambda} \frac{\gamma_\theta}{\kappa_\theta}$ leading to (60) from (83b). □

References

[1] A. J. Collmeyer and S. C. Gupta, "A random sampling approach to the detection of on-off keying," *IEEE Trans. Commun. Technol.*, vol. 10, pp. 678–682, Oct. 1970.

[2] H. G. Feichtinger, K. Grochening, and T. Strohmer, "Efficient numerical methods in non-uniform sampling theory," *Numer. Mathematik*, vol. 69, pp. 423–440, 1995.

[3] G. S. Wagner, "A statistical array processing approach for elastic wavefield data," in *Proc. IEEE Int. Conf. Acoust., Speech, Signal Process. (ICASSP)*, May 1996, vol. 5, pp. 2777–2780.

[4] K. Grochening, "Irregular sampling, Toeplitz matrices, and the approximation of entire functions of exponential type," *Math. Comput.*, vol. 68, no. 226, pp. 749–765, Apr. 1999.

[5] I. F. Akyildiz, W. Su, Y. Sankarasubramaniam, and E. Cayirci, "Wireless sensor networks: A survey," *Comput. Netw.*, vol. 38, no. 4, pp. 393–422, 2002.

[6] A. S. Willsky, "Multiresolution markov models for signal and image processing," *Proc. IEEE*, vol. 90, no. 8, pp. 1396–1458, Aug. 2002.

[7] Y. Jiang, S. Petre, and J. Li, "Array signal processing in the known waveform and steering vector case," *IEEE Trans. Signal Process.*, vol. 52, no. 1, pp. 23–35, Jan. 2004.

[8] N. B. Abdellah, S. S. Crand, J. F. Diouris, and A. A. Ouahman, "Simplified design for digital front end using random sampling in software defined radio architecture," in *Proc. 9th Eur. Conf. Wireless Technol.*, Sep. 2006, pp. 314–317.

[9] R. Verdone, D. Dardari, G. Mazzini, and A. Conti, *Wireless Sensor and Actuator Networks: Technologies, Analysis and Design*. New York, NY, USA : Elsevier, 2008.

[10] V. Potdar, A. Sharif, and E. Chang, "Wireless sensor networks: A survey," in *Proc. Int. Conf. IEEE Adv. Inf. Netw. Appl. Workshops (WAINA)*, 2009, pp. 636–641.

[11] G. Puy, J. P. Marques, R. Gruetter, J. Thiran, D. van de Ville, P. Vandergheynst, and Y. Wiaux, "Spread spectrum magnetic resonance imaging," *IEEE Trans. Med. Imag.*, vol. 31, no. 3, pp. 586–598, Mar. 2012.

[12] W. Chen and I. J. Wassell, "Energy-efficient signal acquisition in wireless sensor networks: A compressive sensing framework," *IET Wireless Sensors Syst.*, vol. 2, no. 3, pp. 1–8, Mar. 2012.

[13] G. Giannakis, F. Bach, R. Cendrillon, M. Mahoney, and J. Neville, "Signal processing for big data," *IEEE Signal Process. Mag.*, vol. 31, no. 5, pp. 15–16, Sep. 2014.

[14] A. Tajer, V. Veeravalli, and H. Poor, "Outlying sequence detection in large data sets: A data-driven approach," *IEEE Signal Process. Mag.*, vol. 31, no. 5, pp. 44–56, Sept. 2014.

[15] A. Sandryhaila and J. Moura, "Big data analysis with signal processing on graphs: Representation and processing of massive data sets with irregular structure," *IEEE Signal Process. Mag.*, vol. 31, no. 5, pp. 80–90, Sept. 2014.

[16] R. K. Ganti, F. Ye, and H. Lei, "Mobile crowdsensing: Current state and future challenges," *IEEE Commun. Mag.*, vol. 49, no. 11, pp. 32–29, Nov. 2011.

[17] A. Faggiani, E. Gregori, L. Lenzini, V. Luconi, and A. Vecchio, "Smartphone-based crowdsourcing for network monitoring: Opportunities, challenges, and a case study," *IEEE Commun. Mag.*, vol. 52, no. 1, pp. 106–113, Jan. 2014.

[18] X. Hu, X. Li, E.-H. Ngai, V. Leung, and P. Kruchten, "Multidimensional context-aware social network architecture for mobile crowdsensing," *IEEE Commun. Mag.*, vol. 52, no. 6, pp. 78–87, June 2014.

[19] P.-Y. Chen, S.-M. Cheng, P.-S. Ting, C.-W. Lien, and F.-J. Chu, "When crowdsourcing meets mobile sensing: A social network perspective," *IEEE Commun. Mag.*, vol. 53, no. 10, pp. 157–163, Oct. 2015.

[20] A. J. Jerri, "The Shannon sampling theorem—Its various extensions and applications: A tutorial review," *Proc. IEEE*, vol. 65, no. 11, pp. 1565–1596, 1977.

[21] E. T. Whittaker, "On the functions which are represented by the expansion if interpolator theory," *Proc. Roy. Soc. Edinburgh*, vol. 35, pp. 181–194, 1915.

[22] V. A. Kotel'nikov, "On the transmission capacity of "ether" and wire in electrocommunications," in *Modern Sampling Theory: Mathematics and Applications*, J. John Benedetto, J. S. G. Paulo Ferreira, Eds. Boston, MA: Birkhäuser Boston, 2001, pp. 27–45.

[23] C. E. Shannon, "Communication in the presence of noise," *Proc. IRE*, vol. 1, no. 37, pp. 10–21, 1949.

[24] H. Landau, "Necessary density conditions for sampling and interpolation of certain entire functions," *Acta Math.*, vol. 117, pp. 37–52, 1967.

[25] K. Groechenig and H. Razafinjatovo, "On Landau's necessary density conditions for sampling and interpolation of band-limited functions," *J. Lond. Math. Soc.*, vol. 54, no. 3, pp. 557–565, 1996.

[26] J. F. Kingman, *Poisson Processes*, 1st ed. New York, NY, USA: Oxford Univ. Press, 1993.

[27] F. A. Marvasti, "Signal recovery from nonuniform samples and spectral analysis on random nonuniform samples," in *Proc. IEEE Int. Conf. Acoust., Speech, Signal Process.*, Tokyo, Japan, 1986, pp. 1649–1652.

[28] J. Hightower and G. Borriello, "Location systems for ubiquitous computing," *IEEE Comput.*, vol. 34, no. 8, pp. 57–66, Aug. 2001.

[29] D. Ganesan, S. Ratnasamy, H. Wang, and D. Estrin, "Coping with irregular spatio-temporal sampling in sensor networks," *2nd Workshop Hot Topics in Networks (HotNets-II)*, Cambridge, MA, USA, Nov. 2003.

[30] J. Li and G. AlRegib, "Rate-constrained distributed estimation in wireless sensor networks," *IEEE Trans. Signal Process.*, vol. 55, no. 5, pp. 1634–1643, May 2007.

[31] J. Li and G. AlRegib, "Distributed estimation in energy-constrained wireless sensor networks," *IEEE Trans. Signal Process.*, vol. 57, no. 10, pp. 3746–3758, Oct. 2009.

[32] S. Cui, J. Xiao, A. Goldsmith, Z.-Q. Luo, and H. V. Poor, "Estimation diversity and energy efficiency in distributed sensing," *IEEE Trans. Signal Process.*, vol. 55, no. 9, pp. 4683–4695, Sep. 2007.

[33] J. Matamoros and C. Antón-Haro, "Optimal network size and encoding rate for random field estimation with wireless sensor networks," in *Proc. 3rd Int. Workshop Comput. Adv. Multi-Sensor Adapt. Process.*, Dec. 2009, pp. 344–347.

[34] F. Ingelrest, G. Barrenetxea, G. Schaefer, M. Vetterli, O. Couach, and M. Parlange, "Sampling and reconstruction of spatial fields using mobile sensors," *ACM Trans. Sens. Netw.*, vol. 6, no. 9, pp. 17:1–17:32, Feb. 2010.

[35] J. Fang and H. Li, "Distributed estimation of Gauss-Markov random fields with one-bit quantized data," *IEEE Signal Process. Lett.*, vol. 17, no. 5, pp. 449–452, May 2010.

[36] M. Nourian, S. Dey, and A. Ahlen, "Distortion minimization in multi-sensor estimation with energy harvesting," *IEEE J. Sel. Areas Commun.*, vol. 33, no. 3, pp. 524–539, 2015.

[37] A. Dogandzic and K. Qiu, "Decentralized random-field estimation for sensor networks using quantized spatially correlated data and fusion-center feedback," *IEEE Trans. Signal Process.*, vol. 56, no. 12, pp. 6069–6085, Dec. 2008.

[38] T. Bouchoucha, M. Ahmed, T. Al-Naffouri, and M.-S. Alouini, "Distributed estimation based on observations prediction in wireless sensor networks," *IEEE Signal Process. Lett.*, vol. 22, no. 10, pp. 1530–1533, 2015.

[39] I. Nevat, G. Peters, and I. Collings, "Random field reconstruction with quantization in wireless sensor networks," *IEEE Trans. Signal Process.*, vol. 61, no. 12, pp. 6020–6033, Dec. 2013.

[40] D. Gu and H. Hu, "Spatial Gaussian process regression with mobile sensor networks," *IEEE Trans. Neural Netw. Learn. Syst.*, vol. 23, no. 8, pp. 1279–1290, Aug. 2012.

[41] D. Dardari, A. Conti, C. Buratti, and R. Verdone, "Mathematical evaluation of environmental monitoring estimation error through energy-efficient wireless sensor networks," *IEEE Trans. Mobile Comput.*, vol. 6, no. 7, pp. 790–802, July 2007.

[42] A. Nordio, C. F. Chiasserini, and E. Viterbo, "Performance of linear field reconstruction techniques with noise and uncertain sensor locations," *IEEE Trans. Signal Process.*, vol. 56, no. 8, pp. 3535–3547, Aug. 2008.
[43] A. Kumar, P. Ishwar, and K. Ramchandran, "High-resolution distributed sampling of bandlimited fields with low-precision sensors," *IEEE Trans. Inf. Theory*, vol. 57, no. 1, pp. 476–492, Jan. 2011.
[44] J. Matamoros, F. Fabbri, C. Antón-Haro, and D. Dardari, "On the estimation of randomly sampled 2d spatial fields under bandwidth constraints," *IEEE Trans. Wireless Commun.*, vol. 10, no. 12, pp. 1750–1761, Dec. 2011.
[45] F. Zabini and A. Conti, "Process estimation from randomly deployed wireless sensors with position uncertainty," *IEEE Globecom*, Houston, TX, USA, Dec. 2011, pp. 1–6.
[46] G. Reise, G. Matz, and K. Grochenig, "Distributed field reconstruction in wireless sensor networks based on hybrid shift-invariant spaces," *IEEE Trans. Signal Process.*, vol. 60, no. 10, pp. 5426–5439, Oct. 2012.
[47] N. Sun and J. Wu, "Optimum sampling in spatial-temporally correlated wireless sensor networks," *EURASIP J. Wireless Commun. Netw.*, vol. 2013, 2013 DOI: 10.1186/1687-1499-2013-5 18 pp.
[48] M. Z. Win, P. C. Pinto, and L. A. Shepp, "A mathematical theory of network interference and its applications," *Proc. IEEE*, vol. 97, no. 2, pp. 205–230, Feb. 2009.
[49] E. Salbaroli, and A. Zanella, "Interference analysis in a Poisson field of nodes of finite area," *IEEE Trans. Veh. Technol.*, vol. 58, no. 4, pp. 1776–1783, May 2009.
[50] M. Haenggi, J. G. Andrews, F. Baccelli, O. Dousse, and M. Franceschetti, "Stochastic geometry and random graphs for the analysis and design of wireless networks," *IEEE J. Sel. Areas Commun.*, vol. 27, no. 7, pp. 1776–1783, Sept. 2009.
[51] Y. Shen and M. Z. Win, "Fundamental limits of wideband localization—Part I: A general framework," *IEEE Trans. Inf. Theory*, vol. 56, no. 10, pp. 4956–4980, Oct. 2010.
[52] A. Rabbachin, A. Conti, and M. Z. Win, "Wireless network intrinsic secrecy," *IEEE/ACM Trans. Netw.*, vol. 23, no. 1, pp. 56–69, Feb. 2015.
[53] B. Lacaze, "La formule d'echantillonnage et A. L. Cauchy," *Traitement du Signal*, vol. 4, no. 15, pp. 289–295, 1998.
[54] F. A. Marvasti, *Non Uniform Sampling: Theory and Practice*. New York, NY, USA: Springer, Jun. 2001.
[55] W. A. Gardner, "A sampling theorem for non-stationary processes," *IEEE Trans. Inf. Theory*, vol. IT-18, pp. 808–809, 1972.
[56] B. Sharma and F. Metha, "A generalized sampling theorem for non-stationary processes," *J. Cybernetics*, pp. 87–95, 1974.
[57] N. Deng, W. Zhou, and M. Haenggi, "The Ginibre point process as a model for wireless networks with repulsion," *IEEE Trans. Wireless Commun.*, vol. 14, no. 1, pp. 107–121, Jan. 2015.
[58] E. Candes, J. Romberg, and T. Tao, "Stable signal recovery from incomplete and inaccurate measurements," *Commun. Pure Appl. Math.*, vol. 59, no. 8, pp. 1207–1223, Aug. 2006.
[59] D. L. Donoho, "Compressed sensing," *IEEE Trans. Inf. Theory*, vol. 52, no. 4, pp. 1289–1306, Apr. 2006.
[60] J. Scarlett, J. Evans, and S. Dey, "Compressed sensing with prior information: Information-theoretic limits and practical decoders," *IEEE Trans. Signal Process.*, vol. 61, no. 2, pp. 427–439, 2013.
[61] Y. C. Eldar, "Sampling and reconstruction in arbitrary spaces and oblique dual frame vectors," *J. Fourier Anal. Appl.*, vol. 1, no. 9, pp. 77–96, Jan. 2003.
[62] D. Stoyan, W. Kendall, and J. Mecke, *Stochastic Geometry and Its Applications*. New York, NY, USA: Wiley, 1996.
[63] M. Z. Win, A. Conti, S. Mazuelas, Y. Shen, W. M. Gifford, D. Dardari, and M. Chiani, "Network localization and navigation via cooperation," *IEEE Commun. Mag.*, vol. 49, no. 5, pp. 56–62, May 2011.
[64] H. S. Shapiro and R. A. Silverman, "Alias-free sampling of random noise," *J. Soc. Ind. Appl. Math.*, vol. 4, no. 8, pp. 225–248, 1960.
[65] F. J. Beutler, "Alias-free randomly timed sampling of stochastic processes," *IEEE Trans. Inf. Theory*, vol. 16, no. 2, pp. 147–152, Mar. 1970.
[66] E. Masry, "Random sampling and reconstruction of spectra," *Inf. Control*, vol. 19, pp. 275–288, Nov. 1971.
[67] E. Masry and M.-C. C. Lui, "Discrete-time estimation of continuous-parameter processes—A new consistent estimate," *IEEE Trans. Inf. Theory*, vol. IT-22, no. 3, pp. 298–312, 1978.
[68] E. Masry, "Poisson sampling and spectral estimation of continuous-time processes," *IEEE Trans. Inf. Theory*, vol. IT-24, no. 2, pp. 173–182, Mar. 1978.
[69] E. Masry, "Alias free sampling: An alternative conceptualization and its applications," *IEEE Trans. Inf. Theory*, vol. IT-24, no. 3, pp. 317–324, May 1978.
[70] E. Masry, "Discrete-time spectral estimation of continuous-time processes the orthogonal series method," *Ann. Math. Statist.*, vol. 8, pp. 1100–1109, 1980.
[71] E. Parzen, "On spectral analysis with missing observations and amplitude modulation," *Sankhya: Ind. J. Statist. A*, vol. 25, no. 4, pp. 180–189, 1963.
[72] E. M. Stein and G. Weiss, *Introduction to Fourier Analysis on Euclidean Spaces*, Princeton, NJ, USA: Princeton Univ. Press, 1971.
[73] A. H. Zemanian, "A generalized Weierstrass transformation," *SIAM J. Appl. Math.*, vol. 15, no. 4, pp. 1088–1105, Jul. 1967.
[74] J. Royo-Álvarez, C. Figuera-Pozuelo, C. Martinez-Cruz, G. Camps-Valls, F. Alonso-Atienza, and M. Martinez-Ramon, "Nonuniform interpolation of noisy signals using support vector machines," *IEEE Trans. Signal Process.*, vol. 55, no. 8, pp. 4116–4126, 2007.
[75] J. Unnikrishnan and M. Vetterli, "Sampling and reconstruction of spatial fields using mobile sensors," *IEEE Trans. Signal Process.*, vol. 61, no. 9, pp. 2328–2340, May 2013.
[76] D. P. Petersen and D. Middleton, "Sampling and reconstruction of wave number-limited function in n-dimensional Euclidean spaces," *Inf. Control*, vol. 5, pp. 279–323, Dec. 1962.
[77] O. A. Z. Leneman, "Random sampling of random processes: Optimum linear interpolation," *J. Franklin Inst.*, vol. 4, no. 281, pp. 302–314, 1966.
[78] O. A. Z. Leneman, "Random sampling of random processes: Impulse processes," *Inf. Control*, no. 9, pp. 347–363, 1966.
[79] O. A. Z. Leneman and J. B. Lewis, "Random sampling of random processes, mean-square comparison of various interpolators," *IEEE Trans. Autom. Control*, vol. AC, no. 11, pp. 396–403, 1966.
[80] A. Papoulis and S. U. Pillai, *Probability, Random Variables and Stochastic Processes*. New York, NY, USA: McGraw-Hill, 2002.

Flavio Zabini (M'13) received the Laurea (*summa cum laude*) in telecommunications engineering and the Ph.D. in electronic engineering and computer science from the University of Bologna, Italy, in 2004 and 2010, respectively.

He is a Researcher at the University of Bologna, Italy. Prior to joining the University of Bologna, he was with the IEIIT-Bo of CNR. In 2004, he has developed his master's thesis at the University of California, San Diego. In 2008, he worked as a visiting student at the DoCoMo Eurolabs of Munich, Germany. In 2013–2014 he was post-doctoral Fellow at German Aerospace Center (DLR), Cologne, Germany. His current research interests include channel coding for free space optical links, echo cancellation for on-channel repeaters, random sampling techniques applied to sensor networks, and performance-fairness trade-off in communication systems.

Andrea Conti (S'99–M'01–SM'11) received the Laurea (*summa cum laude*) in telecommunications engineering and the Ph.D. in electronic engineering and computer science from the University of Bologna, Italy, in 1997 and 2001, respectively.

He is an Associate Professor at the University of Ferrara, Italy. Prior to joining the University of Ferrara, he was with the CNIT and with the IEIIT-Bo of CNR. In Summer 2001, he was with the Wireless Systems Research Department at AT&T Research Laboratories. Since 2003, he has been a frequent visitor to the WCNSL at the Massachusetts Institute of Technology, where he presently holds the Research Affiliate appointment. His research interests involve theory and experimentation of wireless systems and networks including network localization, adaptive diversity communications, cooperative relaying techniques, and network secrecy. He is recipient of the HTE Puskás Tivadar Medal and co-recipient of the IEEE Communications Society's Stephen O. Rice Prize and the IEEE Communications Society's Fred W. Ellersick Prize.

Dr. Conti has served as editor for IEEE journals, as well as chaired international conferences. He has been elected Chair of the IEEE Communications Society's Radio Communications Technical Committee. He is an elected Fellow of the IET and has been selected as an IEEE Distinguished Lecturer.